

DESIGN, FABRICATION, AND CHARACTERIZATION OF AN ACTIVELY-CONTROLLED
MACH 5 TO 8 WIND TUNNEL

A Dissertation Proposal

by

JACOB B. VAUGHN

Submitted to the Graduate and Professional School of
Texas A&M University
in partial fulfillment of the requirements for the degree of
DOCTOR OF PHILOSOPHY

Chair of Committee, Edward White

Committee Members, Rodney Bowersox

Nathan Tichenor

Je Han

Head of Department, Ivett Leyva

March 2024

Major Subject: Aerospace Engineering

Copyright 2024 Jacob B. Vaughn

NOMENCLATURE

Acronyms

ACE	Actively Controlled Expansion
AIAA	American Institute of Aeronautics and Astronautics
AGARD	Advisory Group for Aerospace Research and Development
BCDC	Bush Combat Development Complex
CFD	Computational Fluid Dynamics
FEA	Finite Element Analysis
FEDC	Fischer Engineering Design Center
FOS	Factor of safety
M6QT	Mach 6 Quiet Tunnel
MATLAB	Matrix Laboratory
MDOE	Modern Design of Experiments
MOC	Method of characteristics
MW	Machine Works Inc.
NAHL	National Aerothermochemistry and Hypersonics Laboratory
NASA	National Aeronautics and Space Administration
PID	Proportional Integral Derivative
PLC	Programmable Logic Controller
PSIA	Pounds per Square Inch (Absolute)
RMS	Root Mean Squared
US3D	Unstructured 3D CFD

Common Symbols

A	Area
-----	------

A^*	Nozzle throat area
F	...
K	Proportional Gain Constant
M	Mach number
R	Gas constant
Re'	Unit Reynolds number, $\rho U / \mu$
P	Static Pressure
T	Static Temperature
T_d	Derivative Time Constant
T_i	Integral Time Constant
U	Streamwise Velocity
a	Speed of sound
\dot{m}	Mass flow rate

Greek Symbols

α	Shock angle
ρ	Density
γ	Ratio of specific heats (c_P/c_V)
μ	Dynamic viscosity
θ	Wedge-deflection angle
ξ	Pressure ratio across oblique shock

Common Subscripts

0	Stagnation condition
D	Detachment condition
V	Von Neumann condition
∞	Freestream condition

set

Set condition for PID reference

TABLE OF CONTENTS

	Page
NOMENCLATURE	1
TABLE OF CONTENTS	4
LIST OF FIGURES	6
LIST OF TABLES.....	8
1. INTRODUCTION & LITERATURE REVIEW	1
1.1 Introduction.....	1
1.2 Research Objectives.....	2
1.3 Literature Review	4
1.3.1 Variable Mach-Number Wind Tunnels	4
1.3.2 Parameter Control	5
1.3.3 Flow Quality Characterization and Uncertainty Quantification	7
1.3.4 Hysteresis in Hypersonic Flows	8
2. DESIGN AND FABRICATION OF ACE2.0	9
2.1 Background and Motivation	9
2.1.1 ACE Turbulent Transition.....	9
2.2 ACE2.0 Design	16
2.2.1 Design Requirements.....	16
2.2.2 Nozzle Contour Codes	20
2.2.3 CFD	20
2.2.4 Nozzle and Settling Chamber Design	22
2.2.5 Mechanical Design Iterations	23
2.2.6 20-Ton Linear Actuators Design.....	23
2.2.6.1 Frame Design	23
2.2.6.2 Actuation System Design	23
2.2.6.3 Final Overall Design	24
2.2.6.4 FEA	24
2.3 Fabrication Plans	24
2.3.1 Pressure Test	25
2.3.2 Polishing	25
2.4 Final Assembly, Installation, and Calibration.....	26
2.4.1 Actuation Homing and Calibration	26
2.4.2 Shakedown and First Runs	26

3. EXPERIMENTAL APPROACH & OBJECTIVES	29
3.1 Improved Experimental Control and Efficiency	29
3.1.1 Feedback-Controlled Active Mach Number Variation and Selection	29
3.1.2 Reynolds Number Control Scheme	31
3.2 Freestream Pressure Fluctuation Levels and Uniformity Characterization	34
3.2.1 Freestream Uncertainty Quantification	35
3.2.2 Freestream Hysteresis	38
3.3 Mach Trajectory and Potential Hysteresis Proof of Concept Experiment	38
4. REAMAINING WORK	46
4.1 Maybe.....	46
4.2 Possibly	46
REFERENCES	47
APPENDIX A. ACE2.0 NOZZLE CONTOUR.....	53
APPENDIX B. CFD RESULTS	55
APPENDIX C. ACTUATION SPECIFICATIONS	56
C.1 Appendix Section	56
C.2 Another Appendix Section.....	56

LIST OF FIGURES

FIGURE	Page
1.1 ACE tunnel schematic	5
2.1 ACE nozzle and settling chamber	9
2.2 ACE throat discontinuity	10
2.3 ACE freestream pressure fluctuations in the nozzle exit plane as measured in 2014 ..	12
2.4 ACE freestream pressure fluctuations at various locations as measured ii 2019	13
2.5 ACE freestream pressure fluctuations at 6 inches and 17 inches upstream of nozzle exit as measured in 2022	14
2.6 Mushroom vortex formation at sidewalls	15
2.7 Vertical velocity	16
2.8 Görtler number from ACE nozzle CFD	17
2.9 N-factors for Görtler number in ACE nozzle	18
2.10 Mach lines for noise measured at 17" upstream on nozzle exit.	19
2.11 Comparison of ACE (quadratic) and ACE2.0 (quartic) expansion at throat	21
2.12 Mesh in Pointwise for ACE (top) and ACE2.0 (bottom) nozzle contours.....	21
2.13 ACE2.0 CFD Mach number plot	22
2.14 Comparison of ACE (top) and ACE2.0 (bottom) nozzle and settling chamber designs	23
2.15 Iteration 1 of ACE2.0: Non-active	24
2.16 Iteration 2 of ACE2.0: Sliding Wedge	25
2.17 Iteration 3 of ACE2.0: Rollers.....	25
2.18 Iteration 4 of ACE2.0: Rollers and Actuators	26
2.19 Temporary full CAD design	27
2.20 Manufacturing schedule beginning from September 25, 2023.....	28

3.1	ACE freestream pressure fluctuations.....	35
3.2	Pitot probe measuring 17 inches upstream of nozzle exit.	36
3.3	Flow over wedge resulting in regular reflection of shock	41
3.4	Flow over wedge resulting in Mach reflection of shock.....	42
3.5	Double wedge setup.....	43
3.6	Shock wave reflection configuration domains for Mach number and wedge angle.	44
3.7	Mach-number-varitation-induced hysteresis for 27° wedge	45
A.1	A caption here	54
B.1	A caption here	55
C.1	A caption here	56

LIST OF TABLES

TABLE	Page
3.1 Test matrix for ACE2.0 freestream characterization.....	37

1. INTRODUCTION & LITERATURE REVIEW

1.1 Introduction

In recent decades, the continual improvement in hypersonic aerodynamics has emphasized the need for advancements in wind tunnel ground testing capabilities [1]. Conventional hypersonic wind tunnels rely on distinct fixed nozzle contours to accelerate the flow to the desired Mach number. This approach fixes the Mach number so it only provides a particular flow regime for experiments. Recognizing this, there is a clear need for a continuously variable Mach-number nozzle designed to overcome the limitations of conventional wind tunnels and enable more advanced dynamic hypersonic research.

The objective of this work is to introduce a continuously variable and actively controllable Mach-number nozzle. By dynamically adjusting the throat height and thereby the Mach number throughout the wind tunnel runs, the variable conditions experienced by hypersonic vehicles during different flight trajectories can be effectively modeled. This capability would enable the advancement of ground testing for a more comprehensive understanding of dynamic hypersonic flight and associated phenomena. Furthermore, the active control capability will increase experimental efficiency by allowing measurements at different Mach numbers within a single run and introduce the ability to fine tune the Mach number for improved data quality. However, this variable Mach number capability does introduce the challenge of maintaining desired Reynolds numbers, so feedback control will also be explored for the Reynolds number to counteract this and improve the overall experimental control.

The Actively Controlled Expansion (ACE) wind tunnel at Texas A&M University has served as a workhorse in hypersonic research since 2010 [2–8], and is due for improvements to meet the growing demand of hypersonics research. Although the facility was initially designed to facilitate the continuous variation of Mach number, the mechanical implementation ultimately proved to be cumbersome to adjust. Consequently, the nozzle has remained fixed at Mach 6 for the majority

of the tunnel's operation, falling short of fully realizing its designated variable Mach capability. Additionally, despite the geometry being fixed, the Mach number actually varies throughout a run by up to 5%. Considering this, it is apparent that an update to the ACE nozzle is necessary to remedy these shortcomings.

1.2 Research Objectives

The objectives of this research aim to lay the foundation for continuously variable and actively controlled Mach number capabilities at the National Aerothermochemistry and Hypersonics Laboratory (NAHL). Doing so will expand the current capabilities within the lab for more advanced hypersonic aerodynamics experiments. This will help maintain the NAHL as a cutting-edge national research facility. The existing ACE facility will be upgraded to achieve true active control and to potentially produce low-disturbance flow for higher Reynolds numbers. Its successor, ACE2.0, that is the subject of this work, will employ a feedback-control system with servo motors, linear actuators, and various instrumentation to enable the accurate and continuous variation of Mach number by changing the throat height. Additionally, active feedback-control of the Reynolds number will be developed and potentially implemented.

Once fabricated and calibrated, the ACE2.0 facility will provide:

1. Improved experimental control and efficiency

An active throat height control system will be implemented to enable active feedback-controlled Mach number variation and selection for Mach trajectories and accurate set points. The feedback aspect will attempt to control the Mach number to within 0.5% of the set value. An active control scheme will also be developed to enable feedback-controlled Reynolds number variation and selection that responds to changes in Mach number and stagnation temperature for accurate sweeps and set points. This will allow both constant or varying Reynolds number during a Mach trajectory. The Reynolds number controller will be fully designed but may not be implemented due to constraints.

The control of both of these parameters will yield improved experimental efficiency with

a new capability to explore multiple flow configurations within a single run. Besides enhancing efficiency, the Mach number and Reynolds number control will enable more robust uncertainty quantification and more dynamic experiments that were not possible before. Both of these capabilities are demonstrated in the next objectives.

2. Characterization of freestream flow uniformity and pressure fluctuation levels throughout the nozzle and uncertainty quantification of flow parameters

A flow survey of the nozzle exit plane and centerline will be conducted to measure the freestream flow uniformity and pressure fluctuation levels throughout the nozzle and characterize its performance. This will validate the design and manufacturing of the nozzle and settling chamber and provide a basis for the quality of data gathered in future experiments. A rigorous uncertainty analysis will be performed to quantify the systematic and random uncertainty of the measured flow parameters P , P_0 , and T_0 and the resulting values of Mach number, M , and unit Reynolds number, Re' . This will establish the baseline uncertainty for the freestream flow parameters and enable improved data quality for future experiments. In order to fully characterize the tunnel behavior while actively controlled, an investigation of the potential existence of hysteresis phenomena will be performed. If discovered, any hysteresis will be characterized to fully understand the dynamics of the freestream flow as each parameter is varied.

3. Demonstration of Mach trajectory operation and potential hysteresis in a proof of concept experiment

The capabilities of ACE2.0 will be demonstrated in an experiment that will showcase shock wave interactions between two wedges during a Mach trajectory. This experiment will explore a well-known hysteresis in the transition from a regular reflection to a mach reflection and the ability to produce the phenomenon in this facility.

These objectives will effectively validate and demonstrate the capabilities and merit of the new ACE2.0 facility. In addition, the standard operating procedures for ACE2.0 will be updated to

reflect the best practices deduced throughout the completion of these objectives. The resulting control procedures and interface will be straightforward and well documented so that future users can easily learn to effectively operate the facility. The documentation will not only enhance the accessibility of ACE2.0 for subsequent research endeavors but also contribute to the broader scientific community by providing a robust framework for effective wind tunnel control and dynamic hypersonic vehicle aerodynamics exploration.

1.3 Literature Review

The literature review for this dissertation includes four parts related to hypersonic variable Mach-number wind tunnels and according to the above objectives: (1) variable mach number nozzle design, (2) parameter control, (3) flow quality characterization and uncertainty quantification, and (4) hysteresis in hypersonic flows. This review will discuss articles that establish the most current knowledge base and techniques in the relevant areas of hypersonic wind tunnel research.

1.3.1 Variable Mach-Number Wind Tunnels

Variable Mach number nozzles have been explored in many configurations since the 1950s such as interchangeable fixed-block, plug-type, asymmetric sliding blocks, tilting plate, fully flexible, and hinged/flexure [9]. Each of these designs have varying degrees of flow quality, cost effectiveness, and experimental efficiency that must be considered. Only the fully flexible and flexure designs maximize experimental efficiency without sacrificing flow quality. Of these two, the flexure design minimizes costs by reducing mechanical complexity and supporting structure. Therefore, the flexure design is the optimal choice considering these criteria.

The flexure type nozzle was first proposed in 1955 by Rosen [10] and improved upon separately by Erdmann in 1971 [11] and Rom and Etsion in 1972 [11,12] in order to minimize the mechanical complexity. This simple nozzle design operated by a single jack greatly reduces manufacturing and controls costs and allows for greater flexibility in active control to quickly and continuously vary the Mach number to model dynamic supersonic vehicle flight.

In the last decade, many variable mach number supersonic wind tunnels have been manufac-

tured due to increased demand of hypersonic flight research. The majority of these are fully flexible or flexure nozzle designs with varying implementations of actuation and control [13–21]. All of these facilities were developed to study vehicle flight trajectory and the hysteresis phenomenon therein.

Include paragraph or two about ACE with schematic The ACE tunnel, the facility of interest for this work, has been in operation since 2010 [2–4]. The nozzle is a flexure type that produces Mach 5 to 8 flow in a 9 inch by 14 inch test section. The flexure design is effective in achieving the change in throat height, but it cannot be done continuously and actively during a run. This is the primary issue to be addressed in this work.

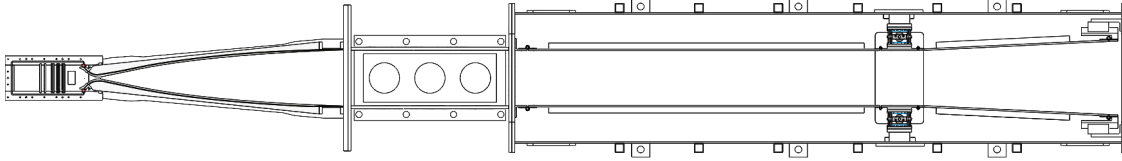


Figure 1.1: ACE tunnel schematic

1.3.2 Parameter Control

A variable Mach number facility requires effective control schemes for the controllable parameters A^* , P_0 , T_0 , and the resulting Mach number, M , and unit Reynolds number, Re' , in order to vary each parameter independently and accurately. This control problem, acknowledged as early as the 1980s, prompted the development of diverse solutions implementing the various areas of control theory such as optimal control [22, 23], state feedback control, mathematical model prediction control, preprogrammed controllers [24], and PID control [25–27].

In recent years, researchers at numerous variable Mach number facilities have embraced advanced intelligent control methods. Techniques such as fuzzy logic, genetic algorithms, neural networks, adaptive control or gain scheduling, and their combinations have been applied [14, 28]. The methods that will be explored in this research are those of Hwang et al. [23], Matsumoto et

al. [24], Ilić et al. [26], and Shahrababaki et al. [14] as they each introduce the different advantages and challenges of each control technique.

Hwang et al. [23] developed a robust LQG/LTR (Linear Quadratic Gaussian with Loop Transfer Recovery) controller enhanced by an anti-integrator windup and a modified Smith predictor to overcome unavoidable modeling errors, uncertainties, and time-delay effects. This controller demonstrated a faster stabilization and exhibited fewer oscillations in comparison to its PID counterpart. Given its superior performance, it presents an appealing prospect for implementation in ACE2.0, and a detailed exploration of this controller will be undertaken in a subsequent chapter.

Matsumoto et al. [24] took a simplified approach by replacing an existing real-time PID controller with a preprogrammed controller to avoid input time delays. This was advantageous for the facility used in that work because the run time was not much longer than the time delay for the PID controller to stabilize. This is the most straightforward approach to obtain specific constant or dynamic trajectories of multiple input parameters but it has limitations. The controller must have a new program for each individual desired parameter set condition or path, and each program must be iterated to minimize errors. Considering these limitations, a preprogrammed controller will be a backup option that will only be explored if necessary. Considering the longer run times of ACE2.0, a PID controller can be implemented with ample time to stabilize.

Ilić et al. [26] implemented a cascade nonlinear feedforward-feedback PID controller as a combined system to enhance a standard single-loop PID. The system's set point reference tracking is improved by the feedforward-feedback architecture, and the disturbance rejection is improved by the cascade architecture. With these two architectures combined in one multi-loop controller, large transient overshoots are eliminated, set point settling times are decreased, and the overall accuracy of the controlled parameters is maximized. Once again, the improved performance of this controller makes it another appealing prospect for ACE2.0, which will be discussed later.

Shahrababaki et al. [14] utilized an artificial neural network and fuzzy logic to enhance a conventional PD controller to handle the complex nonlinearity of the variable mach number wind tunnel flow parameters. The advantages of fuzzy logic include its simplicity and adaptability of

introducing new control rules to handle imprecise data, uncertainty, and unmodeled dynamics. The combined advantage that Shahrabaki et al. explores pertains to the utilization of the neural network to develop the membership functions for the fuzzy logic controller. They designed and trained a feed-forward multilayer perceptron neural network according to the database from the mathematical model of the wind tunnel behavior in order to develop the optimal membership functions. This method will only be explored further for ACE2.0 if the methods of Hwang et al. or Ilić et al. do not yield sufficient performance.

1.3.3 Flow Quality Characterization and Uncertainty Quantification

The primary references regarding flow quality characterization will be the recent AIAA articles by Chou et al. [29] and Duan et al. [30] on hypersonic wind tunnel freestream disturbance measurements. These provide the latest measurement processes and procedures and reference over 50 publications on relevant topics from recent decades. In addition to these two references, a decade of NAHL experience and best practices will guide the characterization of ACE2.0 upon its fabrication and initial shakedown. Key NAHL ACE references on the freestream characterization of ACE are the AIAA paper by Semper et al. [5] and multiple dissertations by Mai [6], Neel [7], and Leidy [8]. Additionally, Leidy performed an uncertainty analysis in the existing ACE tunnel that will provide a rough baseline reference for the uncertainty quantification for ACE2.0.

The primary references for the uncertainty quantification in this research will be the NASA report by Stephens et al. [31], the forthcoming AIAA Guide on Uncertainty Quantification [?], and the dissertation by Curriston [32]. The methodology in this NASA report combines the techniques of the prevalent literature on the subject from the last few decades to quantify the uncertainty of the flow parameters in a supersonic wind tunnel. Curriston's work provides a secondary reference as he thoroughly demonstrates this methodology and that of the forthcoming AIAA guide as a case study in a low speed wind tunnel. The approach described in these references includes a sophisticated treatment of systematic uncertainty using a Mont Carlo method combined with direct comparison of replicate data to characterize random error. Curriston [32] also extensively **treats** pre-test and real-time uncertainly quantification to enhance test campaign quality control and decision support.

1.3.4 Hysteresis in Hypersonic Flows

A review of the literature on hypersonic flow hysteresis yielded many publications discussing shock interactions and inlet start/unstart processes. The inlet start/unstart literature will not be referenced directly in this work but will be valuable for future research in ACE2.0. Focusing on the shock interactions, Hornung et al. [33] first predicted hysteresis in the transition from regular reflection to Mach reflection, but they were unable to experimentally produce the hysteresis effect [34]. Recent literature reveals numerical investigations easily reproduce shock interaction hysteresis [35, 36], while experimental investigations prove more difficult due to the freestream noise in conventional facilities [16, 37]. **Nevertheless, hysteresis has been successfully observed and studied experimentally in open and low-noise (quiet) wind tunnels since 1995 [38].** The two processes that produce hysteresis in the shock interactions are wedge-angle variation and Mach-number variation [39]. Since it is significantly more complex to vary the Mach number, most experimental results are due to the wedge-angle-variation-induced hysteresis [40–44]. However, some research groups with variable Mach number tunnels were able to produce shock interaction hysteresis experimentally by varying the Mach number [15, 45]. Methodologies from the numerical and experimental literature on Mach-number-variation-induced hysteresis will be studied in order to attempt to reproduce shock interaction hysteresis in ACE2.0.

2. DESIGN AND FABRICATION OF ACE2.0

2.1 Background and Motivation

The existing ACE tunnel was designed and manufactured between 2009 and 2010 and began operating in 2010 [2–4]. The nozzle is 40 inches long from the throat to the test section entrance. The test section is 14 inches wide and 9 inches tall. The last 4 inches of the nozzle is a thin flexure portion that allows the throat height to be varied from approximately 0.04 to 0.36 inches, which enables the test-section Mach number to be varied from Mach 5 to 8.

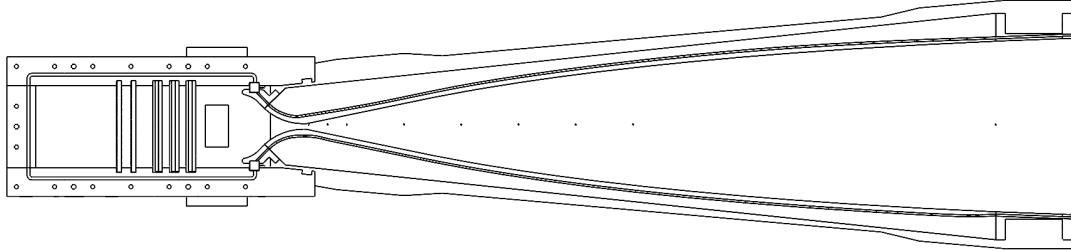


Figure 2.1: ACE nozzle and settling chamber

The original motivation for the redesign was to remanufacture the nozzle to remedy the premature laminar-to-turbulent transition, which is discussed in the next section. However, as the redesign progressed, it became apparent that this was the best opportunity to completely redesign the nozzle and settling chamber to enable active control. This progression and the redesign process is detailed throughout this chapter.

2.1.1 ACE Turbulent Transition

ACE performance data [5–8] shows that below a unit Reynolds number of $Re' = \frac{\rho U}{\mu} \approx 3 \times 10^6 / m$ the RMS pressure fluctuations in the test section are less than 1%, and that above this unit Reynolds number the pressure fluctuation levels significantly increase. It was desired to increase the unit Reynolds number at which laminar flow can be maintained, so the mechanism causing

laminar-to-turbulent transition of the nozzle boundary layers had to be determined. The hypothesis and supporting data regarding the pressure fluctuation levels increase and how it might be delayed to higher unit Reynolds numbers is summarized below.

Five primary suspects for transition were identified:

1. A known manufacturing surface discontinuity at the nozzle throat
2. Sidewall mushroom vortices
3. Görtler vortices
4. Freestream turbulence in the incoming flow and/or upstream boundary layer
5. Wall roughness or waviness

How did lip occur, how big, and where? The throat discontinuity (1) is the result of a decimal truncation error when connecting the subsonic curve to the supersonic MOC contour in Solidworks. The resulting discontinuity can be seen in Figure 2.2, and it has a height of around 0.0003 inches.

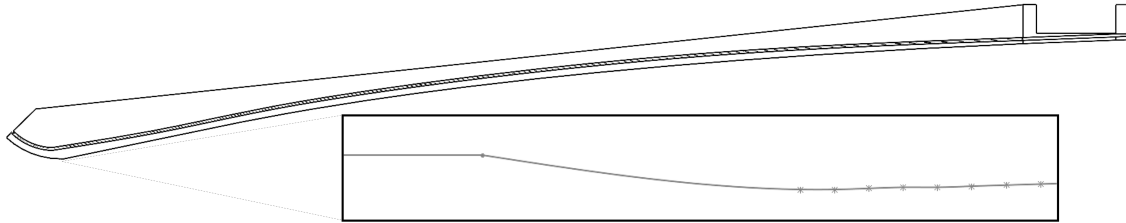


Figure 2.2: ACE throat discontinuity

The sections below evaluate each of these possibilities and support the conclusion that the throat discontinuity is the most likely reason for the increased pressure fluctuations above $Re' \approx 3 \times 10^6/m$. This conclusion is supported by pitot surveys, method-of-characteristics line tracing, and CFD simulations. Sidewall mushroom vortices (2) and Görtler vortices (3) would lead to

transition too far downstream from the throat to be responsible for the pressure fluctuation levels increase. Incoming freestream turbulence (4) and wall surface quality (5) are potential causes of poor flow quality in all supersonic tunnels and are included for completeness. The specific mechanism by which these would cause transition is not known. While item 4 and 5 are not the primary suspects for the pressure fluctuation levels increase, improving these conditions will be addressed in the redesign intended to extend laminar flow to higher unit Reynolds numbers.

ACE Nozzle Noise Surveys

Three recent pitot surveys have been conducted in the ACE tunnel. The first by Mai in 2014 [6] revealed transition occurring around $Re' \approx 3 \times 10^6/m$, as shown in Figure 2.3. The same result was found by Neel in 2019 [7] shown in Figure 2.4 that transition occurs at this Re' value at a location 6 inches upstream of the nozzle exit. A final pitot survey in ACE by Wirth in 2022 (unpublished) was conducted to determine whether the pressure fluctuation levels increase occurred at different Re' values at positions farther upstream in the nozzle. He found pressure fluctuation levels increase at $Re' \approx 3 \times 10^6/m$ at a measurement location 17 inches upstream of the nozzle exit. His results in Figure 2.5 align perfectly with Mai's and Neel's data and clearly establish that the Reynolds number at which pressure fluctuation levels increase is the same at all locations in the nozzle. This suggests that transition is not moving upstream through the nozzle as Reynolds number is increased.

Suspect Mechanism Conclusions

The pressure fluctuation levels revealed the Re' value at which transition occurs but not the transition mechanism. The two mechanisms that were extensively investigated at the start of this work were sidewall mushroom vortices and Görtler vortices. Sidewall mushroom vortices arise from the pressure distribution in the low momentum flow in the sidewall boundary layers. The flow at the centerline expands to the test section pressure ahead of the top and bottom curved walls. The flow at the top and bottom lags behind the centerline flow with a higher pressure to create a vertical pressure gradient that introduces a secondary vertical flow in the sidewall boundary layers

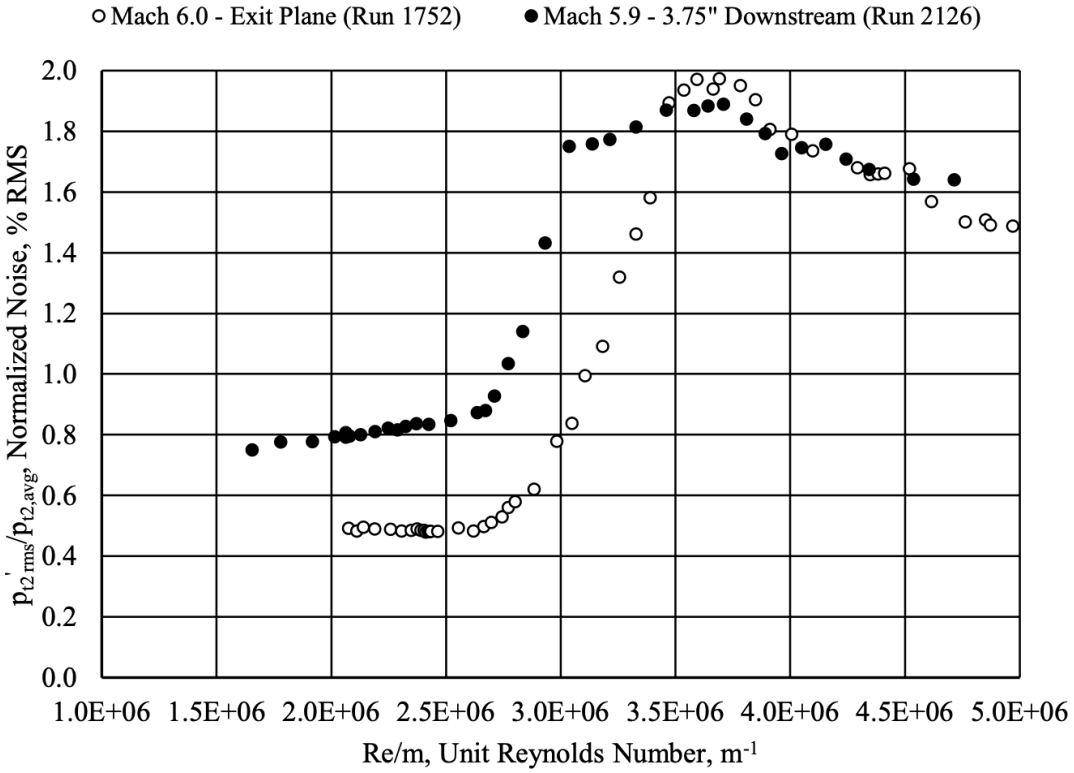


Figure 2.3: ACE freestream pressure fluctuations in the nozzle exit plane as measured in 2014 [6]

that flows from the corners to the centerline [46]. CFD simulations by Kocian (unpublished) show the sidewall mushroom vortices beginning to form approximately 24 inches upstream of the nozzle exit shown in Figures 2.6 and 2.7.

Görtler vortices are counter-rotating streamwise vortices that occur in boundary layers on concave surfaces [47]. To estimate where these may lead to transition, a CFD basic state simulation and N-factor analysis was performed by Kocian in 2022 (unpublished). The results, shown in Figures ?? and ??, indicate that Görtler vortices could induce transition around 8 inches from the nozzle throat. **Elaborate on findings with plots**

Starting here discuss characteristic tracing how plus results and conclusion re: noise, mushroom, Görtler

The origin of the noise measured farthest upstream of the nozzle exit was determined by tracing

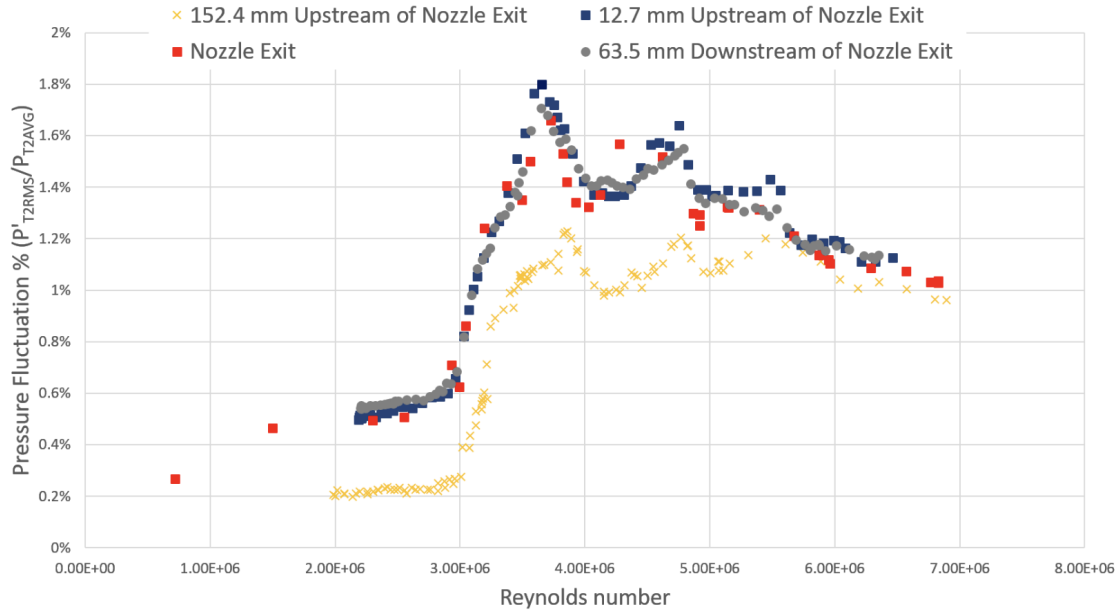


Figure 2.4: ACE freestream pressure fluctuations at various locations as measured in 2019 [7]

characteristic lines from the measurement location at the centerline upstream to the wall. Both the side view and top view of this can be seen in Figure 2.10. **Expand on this with more info. How did you do it? What conclusions did you draw?**

Tracing the characteristics from 17 inches upstream of the nozzle exit, Figure 2.10 shows the origin to be upstream of the throat where sidewall mushroom vortices are not relevant.

However, tracing the characteristics from 17 inches upstream of the nozzle exit, Figure 2.10 shows the measured noise originates at the end of the straight section of the nozzle where Görtler is not relevant.

While both sidewall vortices and Görtler vortices can play some role in transition in planar nozzles, they are no longer considered suspects for the pressure fluctuation levels increase at unit Reynolds numbers above $3 \times 10^6 / \text{m}$.

Rewrite. The combination of pitot surveys and characteristic tracing eliminates the possibility of sidewall mushroom vortices or Görtler vortices because these instabilities would lead to transition downstream of the characteristic wall origins found by tracing from the measurement location

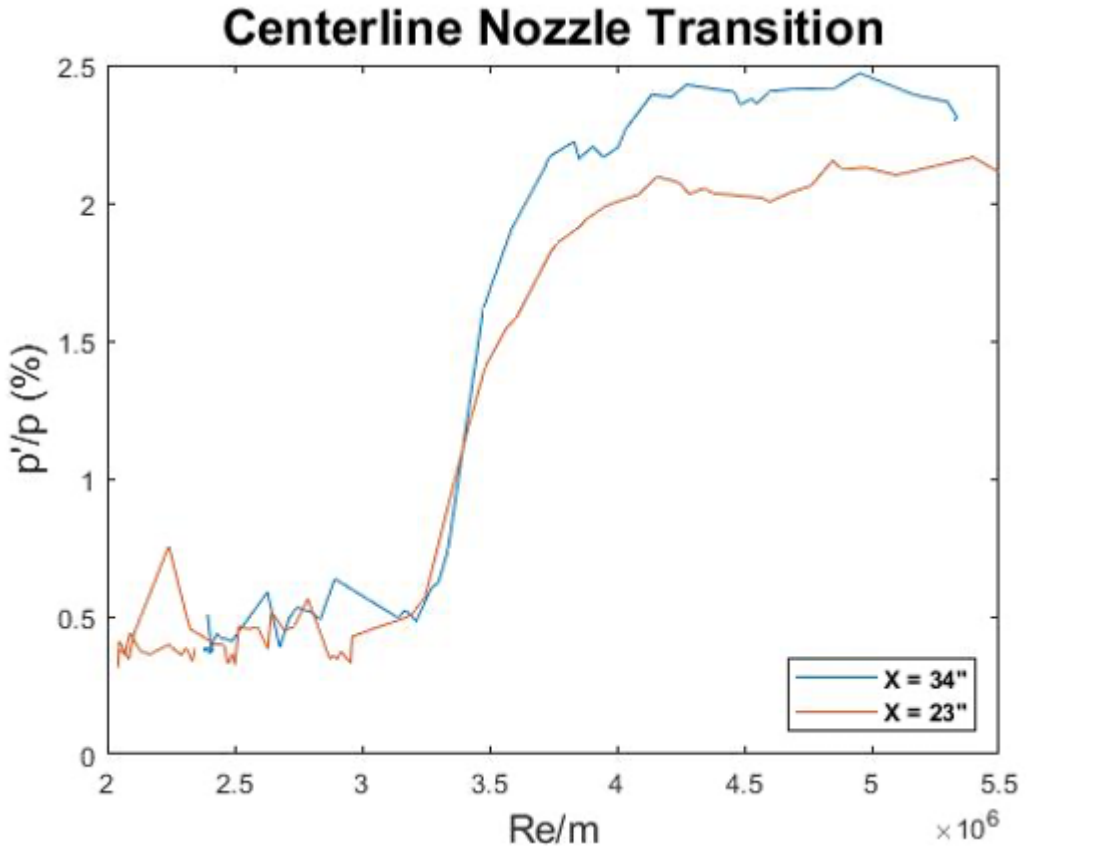


Figure 2.5: ACE freestream pressure fluctuations at 6 inches and 17 inches upstream of nozzle exit as measured in 2022

to the wall intersection. This leaves the surface discontinuity at the throat as the primary culprit for the pressure fluctuation levels increase. The remaining suspect mechanisms are still important to note and address in the redesign of the ACE tunnel.

Following the above conclusions and recommendations, the most likely reason the pressure fluctuations increase is laminar-to-turbulent transition due to a surface discontinuity at the throat. This conclusion is supported by pitot surveys, CFD, and method of characteristics line tracing described above.

Design Recommendations

The following improvements are recommended to maintain laminar flow above $Re' \approx 3 \times 10^6/m$:

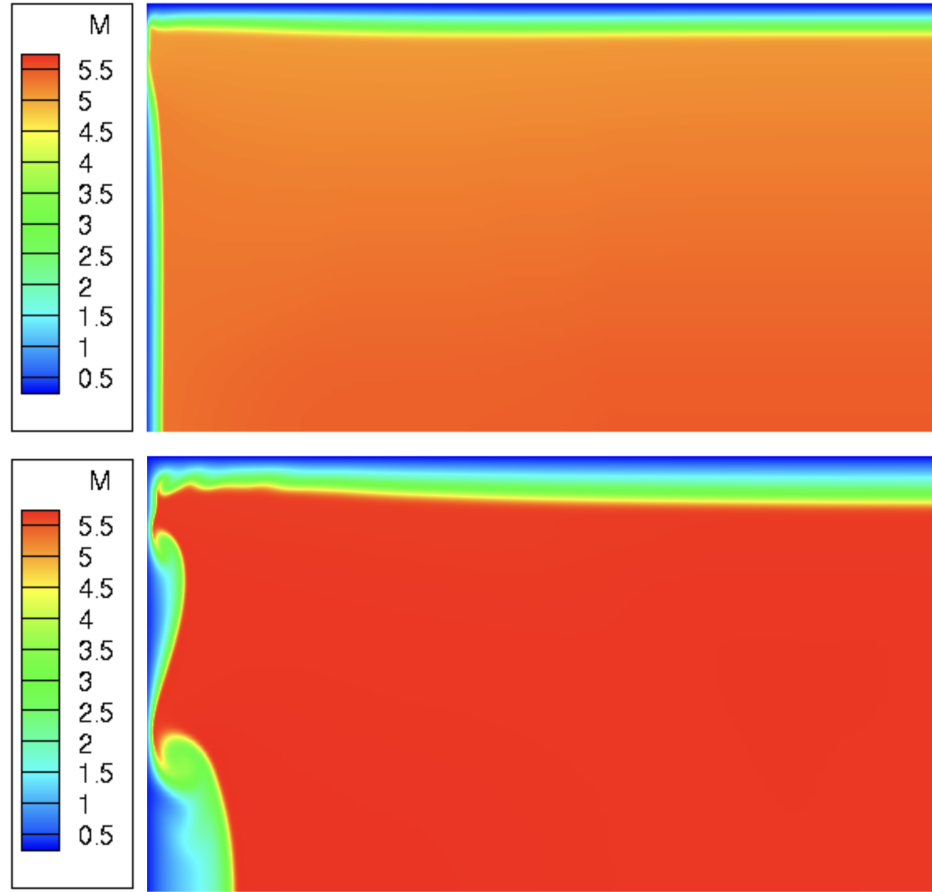


Figure 2.6: Mushroom vortex formation at sidewalls

1. Second-derivative-smooth subsonic-to-supersonic throat transition to eliminate nozzle throat discontinuity
2. Continuous curvature with analytical functions to eliminate waviness and surface discontinuities
3. Enhanced surface polishing to minimize surface roughness
4. Improved settling chamber design to maximize flow uniformity and minimize freestream turbulence upstream of the nozzle throat

Paragraph about future possibility of subsonic boundary layer suction/bleed

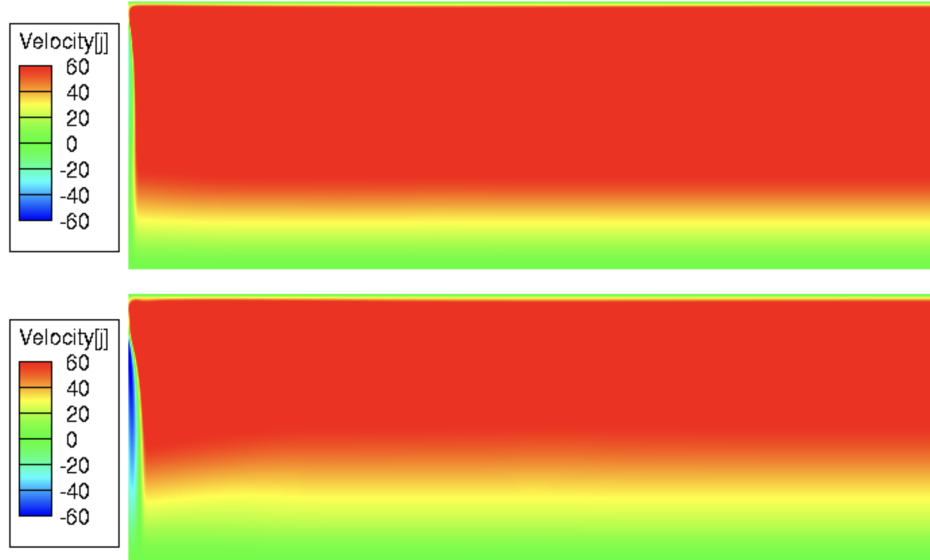


Figure 2.7: Vertical velocity

2.2 ACE2.0 Design

Following these recommendations, the nozzle will be redesigned and remanufactured to meet specific requirements that will ensure the best performance and potentially expand the laminar Reynolds number range. The decision to remanufacture the nozzle presents an opportunity to revise the nozzle and settling chamber design to achieve true active controllability, properly embodying the "ACE" name.

The rest of the chapter details the planned improvements to the ACE tunnel and specific design requirements that will achieve those improvements. In addition to a new nozzle, the settling chamber will also be redesigned to ensure the uniformity and reduce the turbulence of the flow into the nozzle. These improvements are to achieve the goal of increasing the unit Reynolds number at which laminar nozzle flow is maintained.

2.2.1 Design Requirements

ACE2.0 will maintain many characteristics while improving some, so many requirements are the same as the original ACE design. The new tunnel will still produce uniform Mach 5 to 8 flow

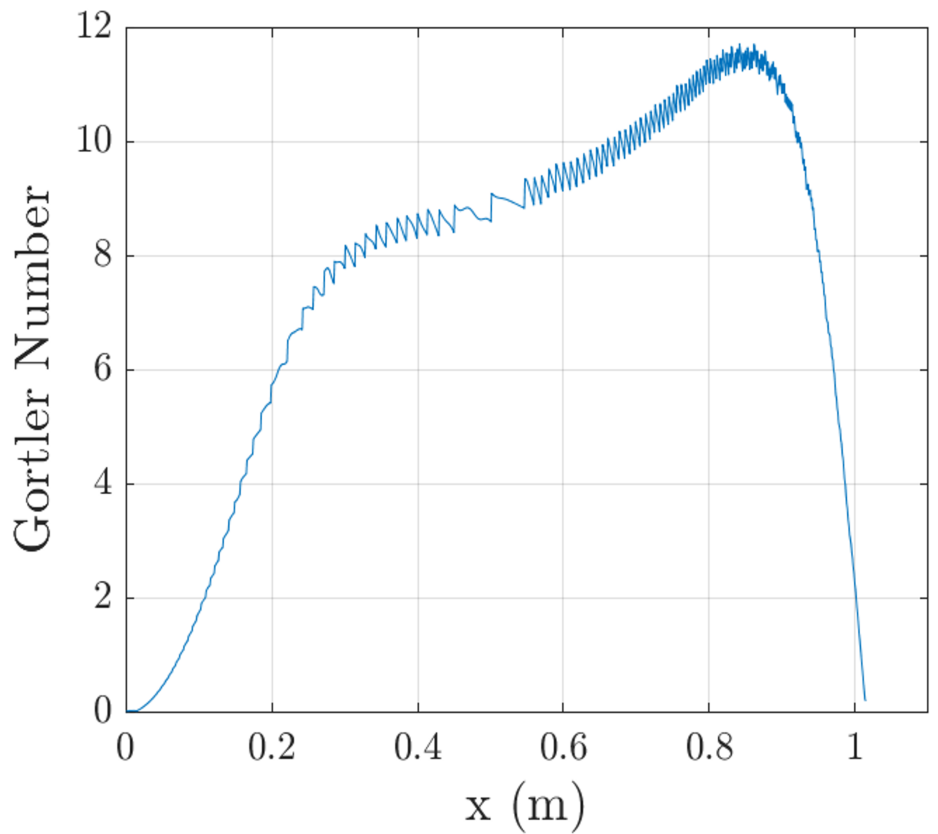


Figure 2.8: Görtler number from ACE nozzle CFD

in the 9 inches by 14 inches test section, withstand a total temperature of 530 K, and maintain a minimum engineering factor of safety (FOS) of 1.5 when operating at a total pressure of 200 psia.

Nozzle Requirements

The current ACE nozzle successfully produces uniform Mach 5 to 8 flow in its core. In order to maintain this good performance and not introduce unknown parameters, the new nozzle will retain a very similar contour with slight improvements. The requirements that remain the same are that the nozzle must produce uniform flow for the entire Mach range, achieve maximum height deflection without exceeding a FOS of 1.5, and prevent leaks up to 200 psia.

The improvements to the nozzle and associated requirements will be a contour with continuous 1st and 2nd derivatives that is specified by analytical functions that will eliminate discontinuities and truncation error and a maximum allowable stress less than or equal to that found in the current

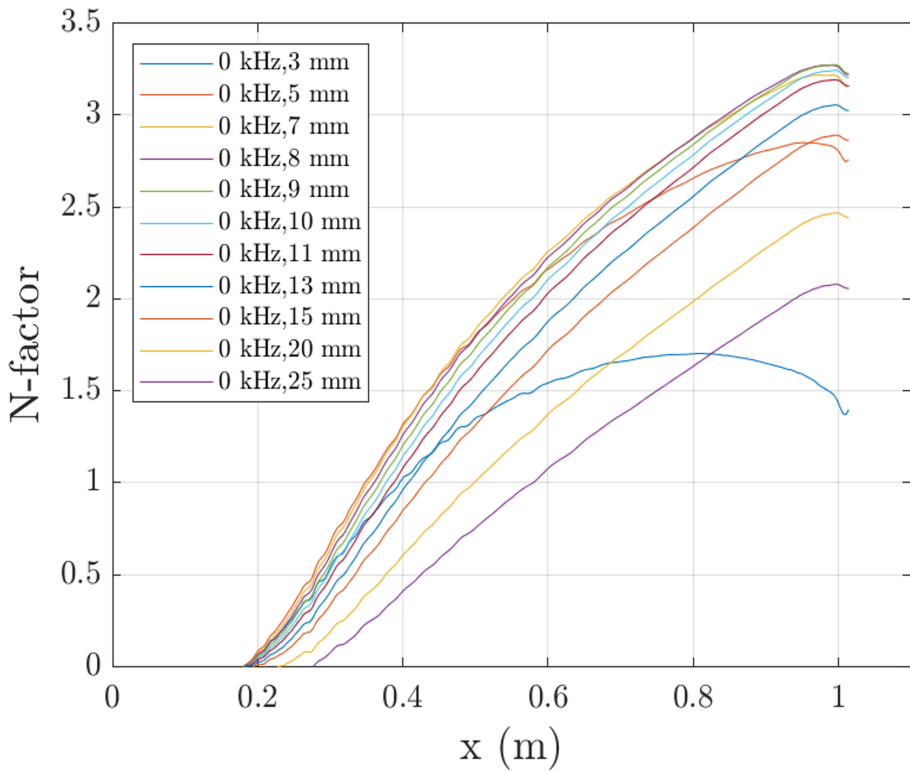


Figure 2.9: N-factors for Görtler number in ACE nozzle

ACE flexure at maximum deflection.

Settling Chamber Requirements

The current ACE settling chamber design provides multiple opportunities to improve flow conditioning and ease of maintenance. The new settling chamber design will increase the length and height and allow for variable aerogrid/screen configurations. The requirements that remain the same are low freestream turbulence, thin stable wall boundary layers, maximum uniformity, and preventing leaks at a pressure of 200 psia. The implementation of these requirements will be improved in the new design to achieve improved incoming flow into the nozzle.

Following Reshotko et al. [48], the length of the settling chamber shall accommodate a separation of 250 characteristic mesh sizes between screens allowing for adequate turbulence decay. The aerogrids will have a hexagonal perforation pattern to increase porosity and decrease pressure loss. The number of aerogrids and screens shall be variable to allow for future flow conditioning

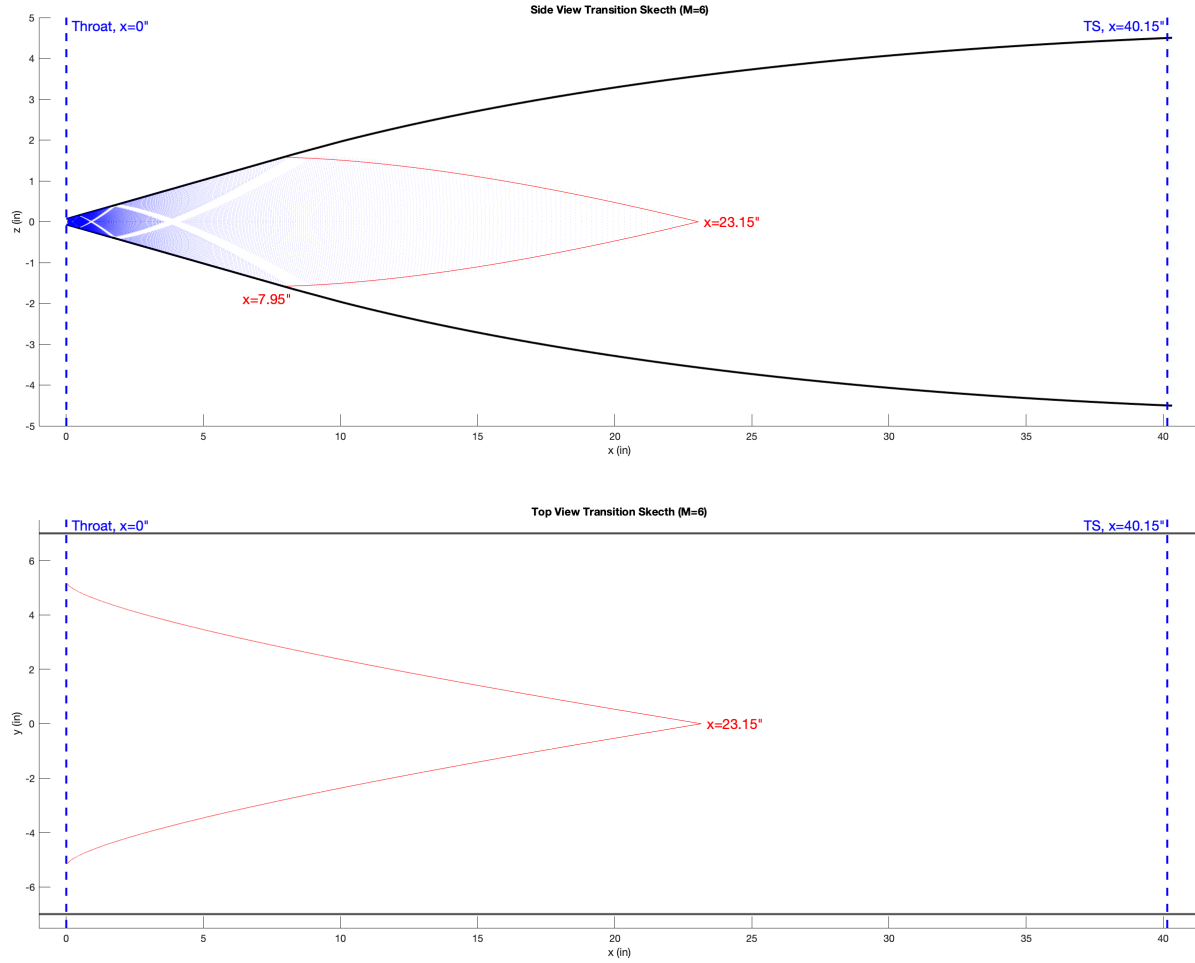


Figure 2.10: Mach lines for noise measured at 17" upstream on nozzle exit.

experiments. The inlet shall include a baffle system that will provide an acceptable initial distribution and mixing of the air received from the high-pressure inlet piping. The overall design will accommodate the option for future boundary layer suction slots.

A settling chamber height of 6 inches was chosen to keep the velocity as slow as possible without going below 10 ft/s for the majority of the Mach number range, according to Pope and Goin [49]. The reason for this minimum is to prevent thermal convection vortices from dominating the flow at the walls. The interior of ACE2.0 will also be heated prior to the start of the run to help avoid thermal gradients.

2.2.2 Nozzle Contour Codes

The multiple reflections method-of-characteristics (MOC) Fortran script written by Bowersox that produced the ACE nozzle contour was used for the new nozzle contour. In order to achieve continuous first and second derivative continuity, a section of the code was modified to produce a fourth-order expansion section instead of the original second-order curve. This allowed the expansion section to match the curvature of both the subsonic section and the straight section. The code modification is included in Appendix A, and a comparison of the original quadratic and the new quartic expansion sections is shown in Figure 2.11. In this figure, the ACE contour is directly from the MOC points and the ACE2.0 contour is specified by an analytic fourth-order polynomial. The waviness of the MOC points can be seen here, emphasizing the need to define the entire nozzle with analytic functions.

After the MOC points were produced by the Fortran script, they were imported into a MATLAB script to fit with analytic functions. The subsonic curve is given by a fifth-order polynomial with six boundary conditions of $y(-L) = H$, $y'(-L) = 0$, $y''(-L) = 0$, $y(0) = h$, $y'(0) = 0$, and $y''(0) = 0$. **These condition require the nozzle contour...** The straightening section is given by a function found using the `lsqcurvefit` function with a combination of power and logarithmic functions in MATLAB. The equations for each section are given in Appendix A.

2.2.3 CFD

In order to verify the above nozzle contour performance compared to the original ACE contour, both contours were simulated in 2D CFD. First, a mesh was created in Pointwise for each contour with 400 equally spaced columns of cells in the x-direction. Each column had the spacing scaled to accurately capture the boundary layer with the smallest cell height around 4×10^{-6} inches at the curved wall and the largest around 0.2 inches at the centerline as seen in Figure 2.12. The CFD analysis was performed at a time when the settling chamber design was still at a height of 9 inches, so the analysis will be performed again to validate the 6 inch.

After creating a mesh for each, they were simulated using US3D on the Texas A&M super-

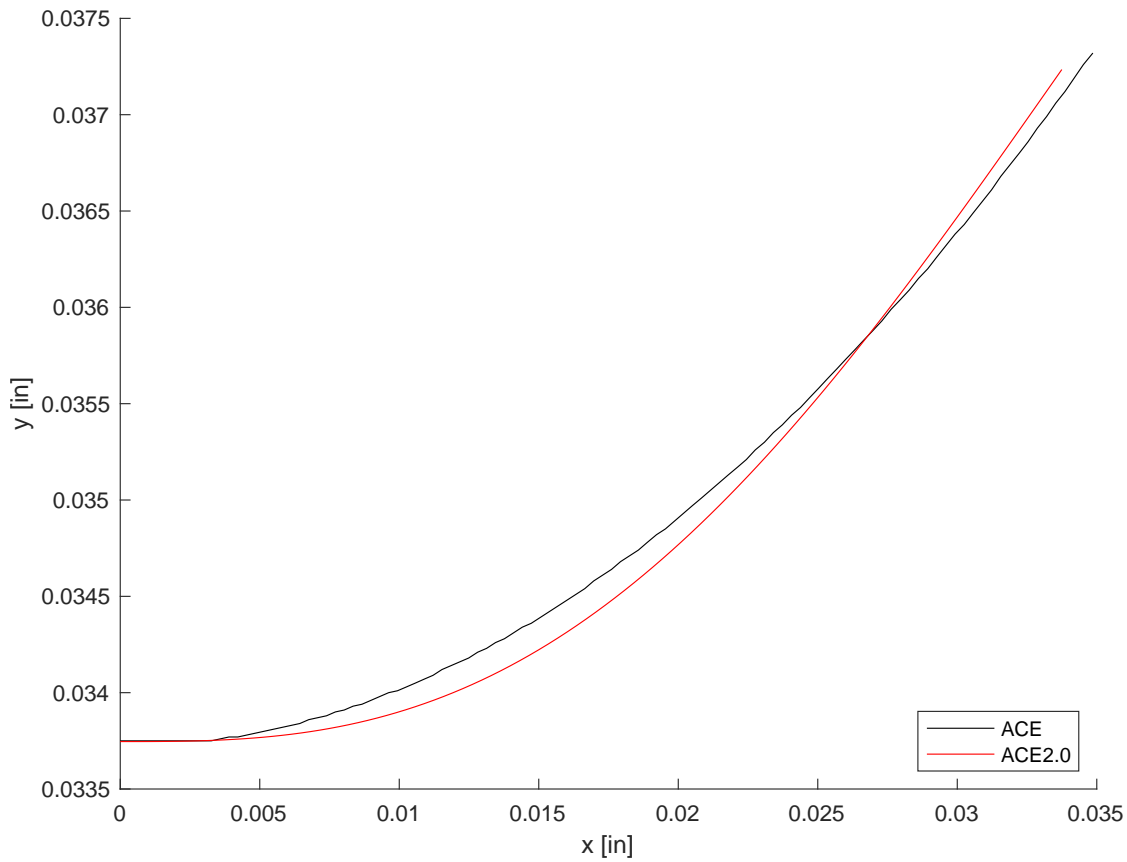


Figure 2.11: Comparison of ACE (quadratic) and ACE2.0 (quartic) expansion at throat

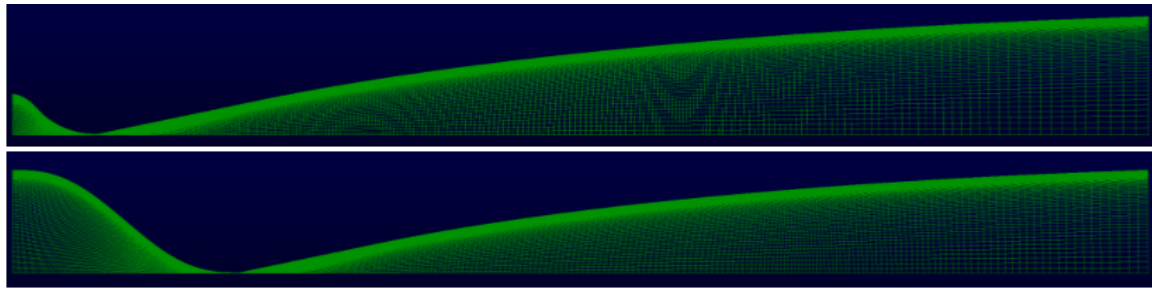


Figure 2.12: Mesh in Pointwise for ACE (top) and ACE2.0 (bottom) nozzle contours

computer, Grace. **Stuff about inputs and convergence conditions followed by some results**

A sample of the results is shown in Figure 2.13. The full ACE2.0 CFD results compared to ACE is given in Appendix B.

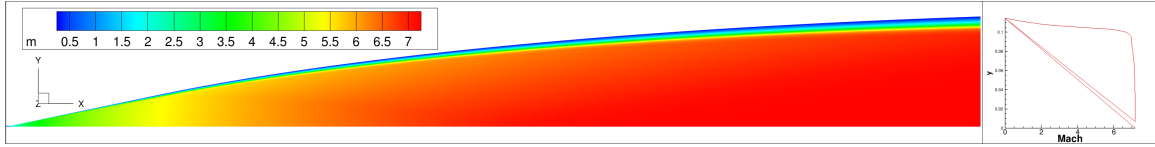


Figure 2.13: ACE2.0 CFD Mach number plot

2.2.4 Nozzle and Settling Chamber Design

The resulting contour from above was imported into Solidworks using the analytic equations given in Appendix A, and the new ACE2.0 nozzle and settling chamber were designed following the above requirements. In order to accommodate the active control, the nozzle and settling chamber were combined into single rigid upper and lower pieces. Similar to ACE, the last 4 inches of the nozzle is a separate flexure piece to enable the variable Mach number capability. The overall length of the nozzle and settling chamber was increased by 19 inches with most of the added length contributed to the settling chamber.

The settling chamber is 1.7 inches taller and has a few considerable improvements. The flow conditioners are enclosed in a standalone box that allows for easy maintenance and future modifications of screen configurations. The initial configuration provides 3 inches between each aerogrid and screen for adequate turbulence decay. Inlet flow spreaders are added as well to allow uniform mixing of the incoming air before flowing through the aerogrids.

The ACE design had the relative motion interface between nozzle and settling chamber with a large rubber seal that struggled to properly seal at higher Mach numbers. For ACE2.0, the end of the settling chamber is split into two pieces to allow the rotation of the nozzle blocks. This moves the potential sealing issue upstream of the flow conditioners where minor leaks are much less of a concern. The final ACE2.0 nozzle and settling chamber design compared to ACE is shown in Figure 2.14.

All of the nozzle and settling chamber parts will be made from 304 stainless steel except for the flexures, which will be made from Condition A 17-4 PH stainless steel for maximum strength while maintaining flexibility.

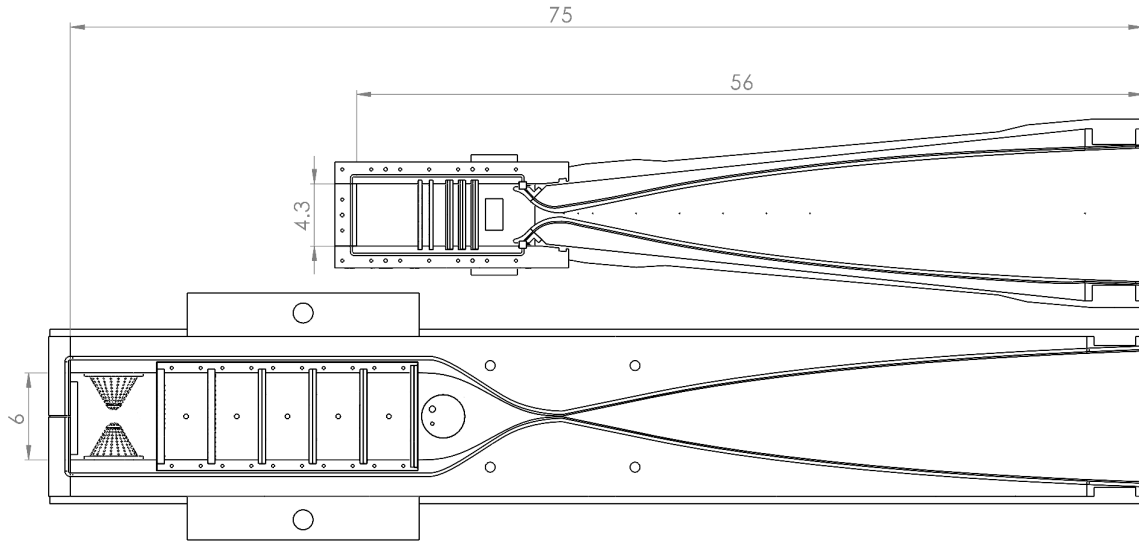


Figure 2.14: Comparison of ACE (top) and ACE2.0 (bottom) nozzle and settling chamber designs

2.2.5 Mechanical Design Iterations

There were a few distinct iterations throughout the design process of ACE2.0 that are worth mentioning briefly. As mentioned, the original intent of the ACE redesign was not to enable active control, so the initial mechanical design was limited.

2.2.6 20-Ton Linear Actuators Design

The final iteration...

2.2.6.1 Frame Design

Description and figures

Originally planned to water jet bars from brace stock to save material cost and reduce excess. Later discovered that the cost of time and tooling on water jet to cut all pieces from 3 inch 4140 allot steel exceeds the cost of ordering bar stock.

2.2.6.2 Actuation System Design

Detailed specifics of actuation components

The actuation system will comprises 20-ton linear actuators, 20:1 gearboxes, servo motors, and

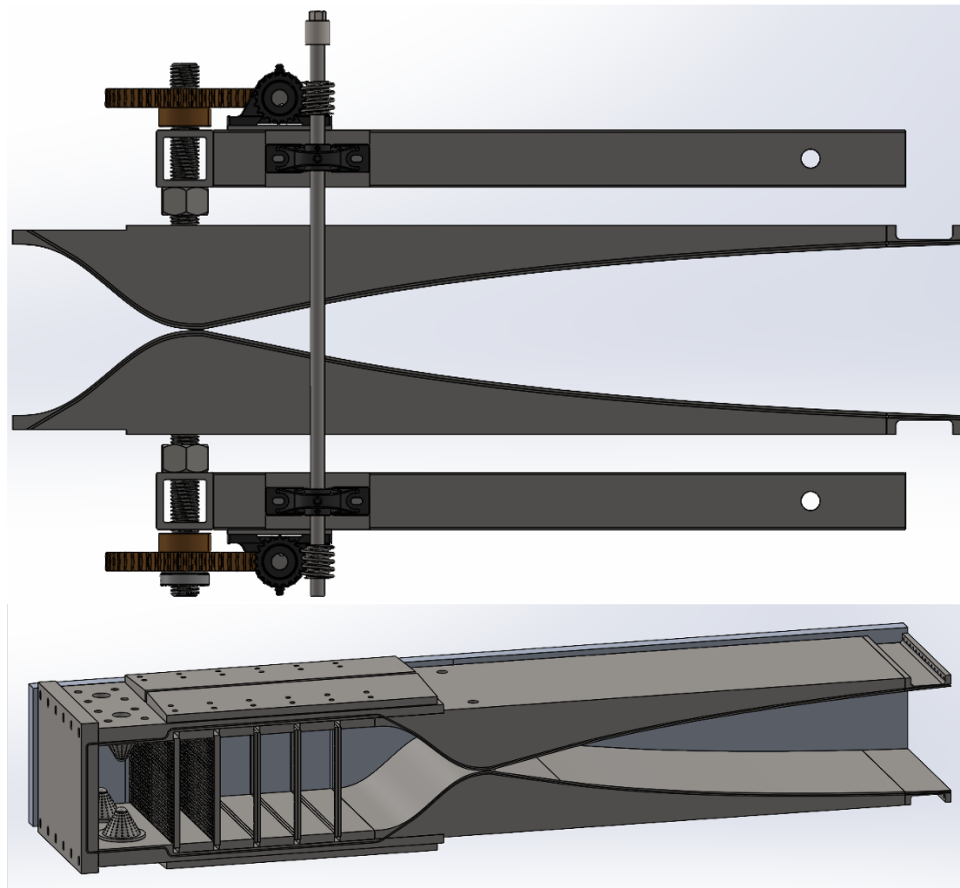


Figure 2.15: Iteration 1 of ACE2.0: Non-active

a PLC to receive feedback inputs and control the system.

2.2.6.3 Final Overall Design

The entire design will integrate with the existing ACE test section and other infrastructure.

Pictured below is the final overall ACE2.0 assembly.

2.2.6.4 FEA

Stress and FOS stuff with figures

2.3 Fabrication Plans

How much to detail? Pictures of stock? What parts to show final machined?

ACE2.0 is currently being fabricated. Most machining is completed. Pictures of machining

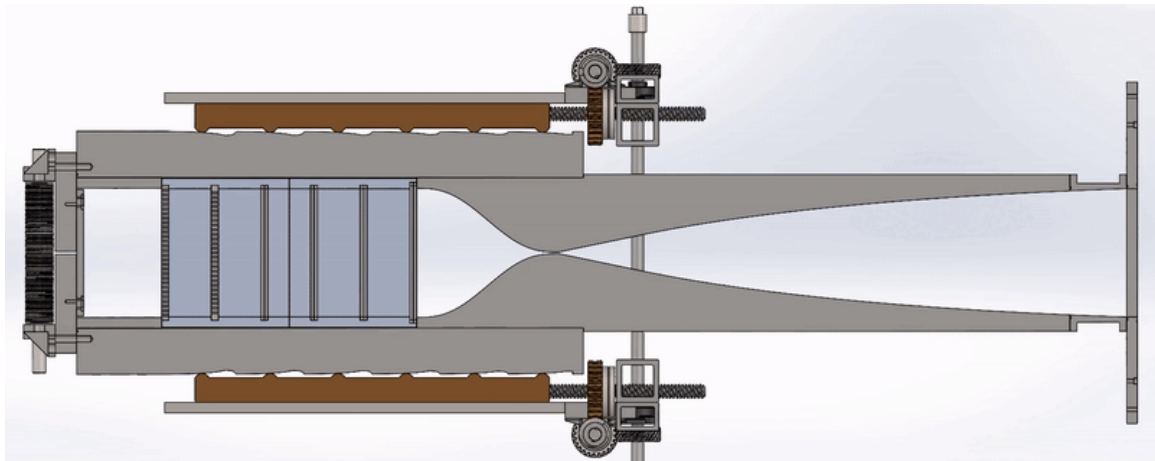


Figure 2.16: Iteration 2 of ACE2.0: Sliding Wedge

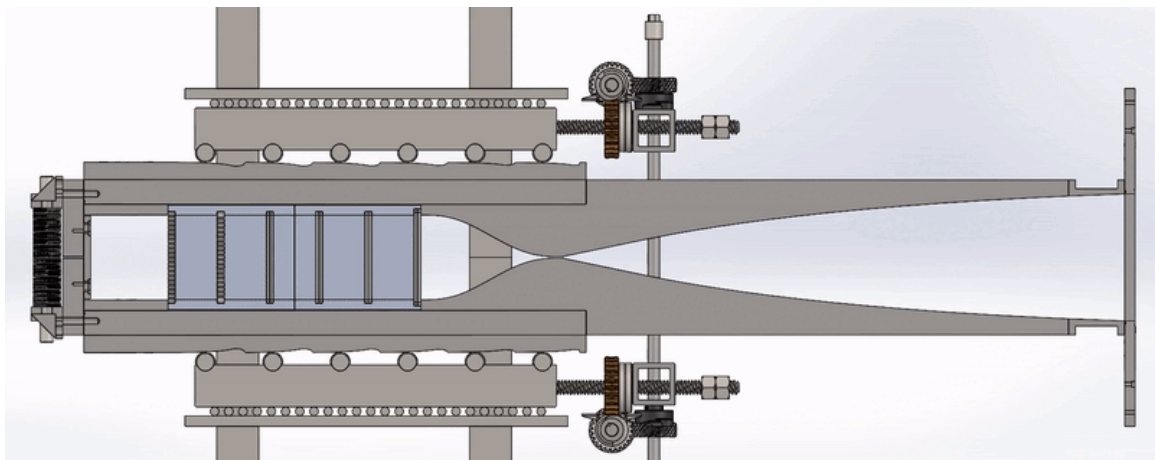


Figure 2.17: Iteration 3 of ACE2.0: Rollers

and fabrication.

2.3.1 Pressure Test

Check structural integrity at 200 psia and evaluate sealing.

2.3.2 Polishing

Astro Pak polishing nozzles and sidewalls to 1 Ra.

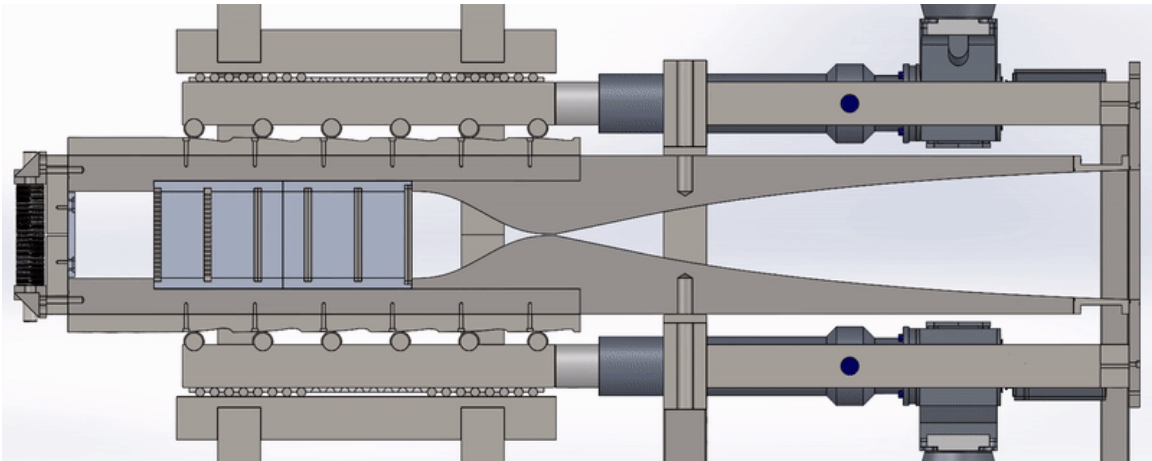


Figure 2.18: Iteration 4 of ACE2.0: Rollers and Actuators

2.4 Final Assembly, Installation, and Calibration

The final assembly will occur at the NAHL. Once nozzles and actuators are assembled in the frame, ACE2.0 will be rolled into the lab to replace ACE. All hoses, wires, and instrumentation attached to the nozzle and settling chamber will be removed and ACE will be rolled out of the lab. ACE2.0 will roll in and reconnect all hoses, wires, and instrumentation.

2.4.1 Actuation Homing and Calibration

Before the sidewalls are installed, the nozzles will be aligned by homing the servo motors with the limit switches. At this point shims will be used to make fine adjustments to limit switch positions to ensure a minimum Mach number of **4.9** and a maximum Mach number of **8.5**.

2.4.2 Shakedown and First Runs

Decide what the first runs' purposes should be to properly calibrate.

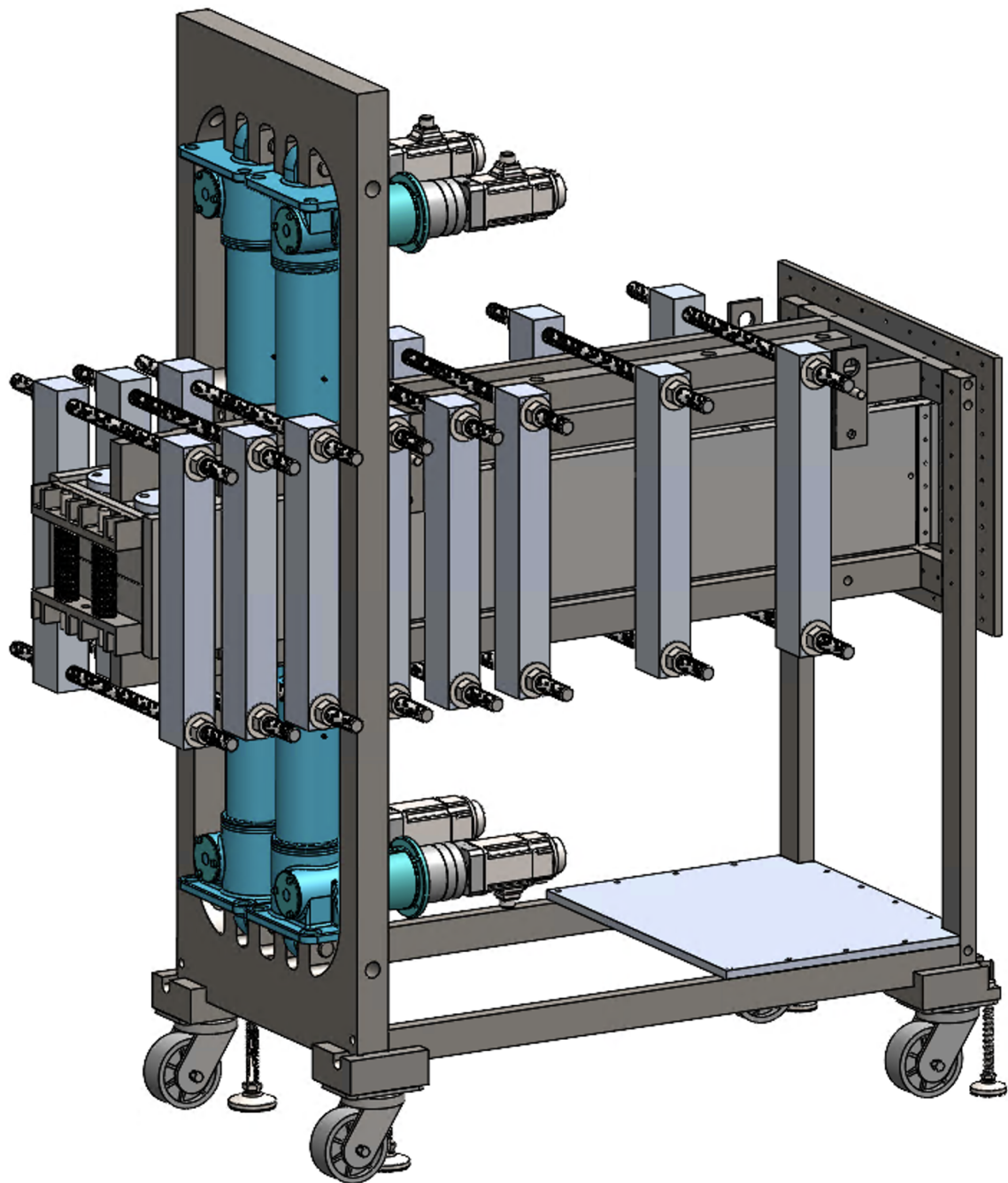


Figure 2.19: Temporary full CAD design

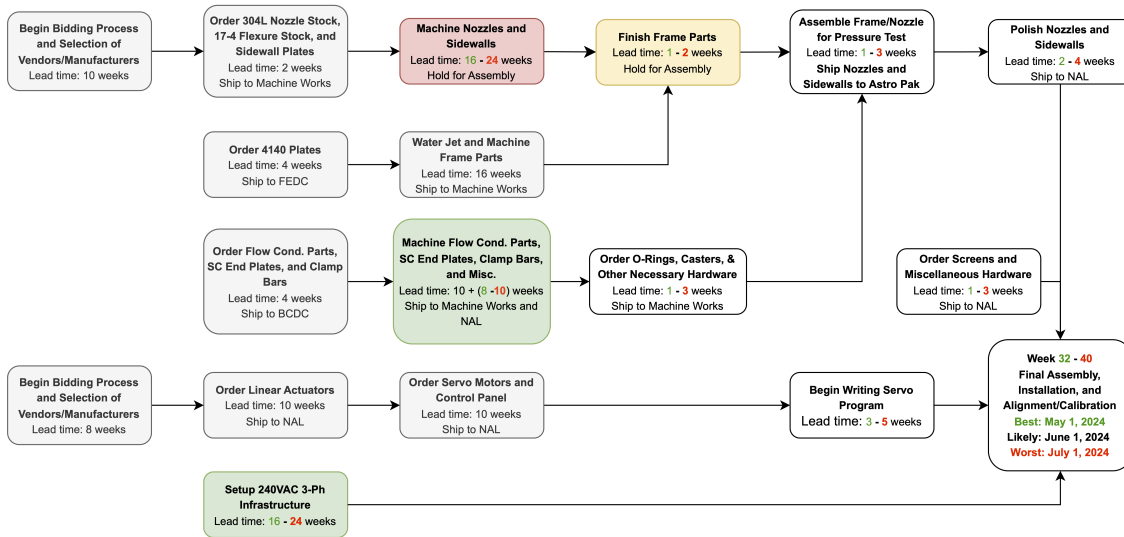


Figure 2.20: Manufacturing schedule beginning from September 25, 2023.

3. EXPERIMENTAL APPROACH & OBJECTIVES

Following the completed installation and calibration discussed above, each of the three primary objectives will be accomplished or demonstrated sequentially. First, the improved experimental control and efficiency as a result of the above ACE2.0 design will be demonstrated by establishing and verifying the feedback-controlled active Mach variation and selection capability as well as the Reynolds number control scheme, if implemented. Second, the freestream flow produced by the calibrated nozzle will be characterized in terms of freestream flow uniformity and pressure fluctuation levels with uncertainty quantification and an exploration hysteresis. Third, the flow parameter control capabilities will be demonstrated in a proof of concept experiment of shock interactions during a Mach trajectory and any potential hysteresis exhibited. As a result of this work, the foundation will be set for future researchers to explore dynamic hypersonic aerodynamic in a more sophisticated and efficient manner with the control capabilities of ACE2.0.

3.1 Improved Experimental Control and Efficiency

The overall objective here is to establish and substantiate the mechanisms of ACE2.0 that allow greater control of the tunnel input parameters for both more efficient and dynamic experiments. The primary design objective of ACE2.0 was to enable active Mach number control during a run, which alone provides many key experimental advantages. However, there is still much to be desired with the parameter control capabilities to achieve full aerodynamic similarity for any flight trajectory. Thus, more precise control methods for Mach number and Reynolds number will be explored through the following objectives.

3.1.1 Feedback-Controlled Active Mach Number Variation and Selection

As stated, the primary design objective of ACE2.0 was to enable active control of the Mach number, but this capability will be taken one step further to accurately maintain the desired Mach number once set. During a tunnel run, the Mach number may vary because both pressure and thermal loads can cause the throat height to vary. Current experience shows that the Mach number

can vary by up to 5%. The goal of this work is to implement active feedback control and reduce this error to less than 0.5%.

The general approach for this feedback control is straightforward by designing a PID controller with an input of the measured Mach number and output of actuator position or velocity. The measured Mach number is calculated from the measured stagnation pressure and static pressure by solving the isentropic relation:

$$M = \sqrt{\frac{2}{\gamma - 1} \left[\left(\frac{P_0}{P} \right)^{\frac{\gamma-1}{\gamma}} - 1 \right]} \quad (3.1)$$

The relationship between the throat height and the Mach number is given by:

$$\frac{A_*}{A} = M \left[\left(\frac{2}{\gamma + 1} \right) \left(1 + \frac{\gamma - 1}{2} M^2 \right) \right]^{-\frac{\gamma+1}{2(\gamma-1)}} \quad (3.2)$$

This is then subtracted from the set throat height to get the error signal for the PID transfer function:

$$E(s) = h_{\text{set}} - H(s) \quad (3.3)$$

There are many design options for PID controllers depending on the desired performance characteristics. The standard approach is simply a PI controller due to the derivative action amplifying measurement noise and potential causing instability [25]. However, the derivative effect of limiting overshoot and settling time is desirable, so it will not be neglected entirely. One final option is to add high frequency filtering into the derivative term to mitigate the effects of measurement noise. Each of these options will be explored, and the following equations show the transfer functions for

PI, PID, and PID with high frequency noise filtering respectively:

$$G(s) = \frac{H(s)}{E(s)} = K \left(1 + \frac{1}{T_i s} \right) \quad (3.4a)$$

$$= K \left(1 + \frac{1}{T_i s} + T_d s \right) \quad (3.4b)$$

$$= K \left(1 + \frac{1}{T_i s} + \frac{T_d s}{1 + \frac{T_d s}{N}} \right), \quad N = 2 \text{ to } 20 \quad (3.4c)$$

In practice, the Sysmac software used to write the logic for the PLC has a built-in PID function with gain autotuning capability. This will be explored in detail first in simulations in Sysmac followed by active tests in ACE2.0. This built-in PID loop will be used permanently if the resulting Mach number control is sufficient. Otherwise, the PID controller described above will be fully developed and implemented. In either case, a gain schedule will also be developed to modify the controller response throughout the Mach range to best handle the nonlinearity of the throat height and Mach number relationship.

3.1.2 Reynolds Number Control Scheme

In subscale model experiments, the Reynolds number plays an important role in maintaining similarity with real-world situations. Controlling the Reynolds number more effectively will enable more accurate and intentional experiments. The primary goal of this objective is to provide a feedback control scheme that allows the Reynolds number to be held at a set value that is either constant or dynamic. For the purposes of this discussion, any mention of the Reynolds number will be referring to the unit Reynolds number, $Re' = \frac{\rho U}{\mu}$.

The main control parameter for Reynolds number will be the settling chamber stagnation pressure. The Reynolds number is coupled with respect to pressure, temperature, and Mach number. The goal will be to control the stagnation pressure to counteract changes in both temperature and Mach number. For reference, the settling chamber stagnation temperature typically increases during a run by up to 40 K, and, of course, the Mach number can vary between 5 and 8. The effect of temperature will be examined during both simulations and experiments to determine if a more ad-

equate control system is required to maintain constant temperature or if this effect on the Reynolds number can be compensated by changing the pressure.

A mathematical model will be developed to be implemented for future physical PID control of the pressure regulator and the Reynolds number as a result. The physical implementation of this controller in this work will be dependent on budget and schedule constraints. The primary constraint here will be the ability to quickly replace the existing regulator manual valve control with a controlled valve. The M6QT utilizes the same air supply infrastructure, so any complications throughout the valve replacement process would result in both facilities being inoperable and a delay in all planned research for this work and others.

One other factor to be considered in the stagnation pressure control is the time response delay due to both the distance between the regulator and the tunnel and the maximum operating speed of the regulator. The distance from the regulator to the settling chamber inlet is around 7 meters, resulting in a maximum response time of **140 milliseconds with a minimum pipe flow velocity of $v_{pipe,min} = \dot{m}_{min}/\rho/A_{pipe} \approx 50 \frac{m}{s}$** . The maximum regulator operating speed is...

The following derivation provides a starting point for the mathematical model.

begin{fix equations}

$$Re' = \frac{\rho U}{\mu} \quad (3.5)$$

$$\frac{T_0}{T} = \left(1 + \frac{\gamma - 1}{2} M^2\right) = F \quad (3.6)$$

$$\frac{P_0}{P} = \left(1 + \frac{\gamma - 1}{2} M^2\right)^{\frac{\gamma}{\gamma+1}} = F^{\frac{\gamma}{\gamma+1}} \quad (3.7)$$

$$\rho = \frac{P}{RT} = \frac{P_0 F^{\frac{-\gamma}{\gamma-1}}}{RT_0 F^{-1}} = \frac{P_0}{RT_0 F^{\frac{1}{\gamma-1}}} \quad (3.8)$$

$$U = M \sqrt{\gamma RT} = M F^{-\frac{1}{2}} \sqrt{\gamma RT_0} \quad (3.9)$$

$$Re' = \frac{\rho U}{\mu} = \frac{1}{\mu} \frac{P_0}{RT_0 F^{\frac{1}{\gamma-1}}} M F^{-\frac{1}{2}} \sqrt{\gamma RT_0}$$

$$Re' = \sqrt{\frac{\gamma}{RT_0}} \frac{MP_0}{\mu} F^{-\frac{\gamma+1}{2(\gamma-1)}} \quad (3.10)$$

Differentiating Re' assuming γ and R are constant and with $\frac{dF}{dt} = (\gamma - 1)M \frac{dM}{dt}$ gives:

$$\frac{d(Re')}{dt} = P_0 \frac{dM}{dt} + M \frac{dP_0}{dt} - \frac{MP_0}{\mu} \frac{d\mu}{dt} - \frac{\gamma+1}{2} M^2 P_0 F^{-1} \frac{dM}{dt} \quad (3.11)$$

Sutherland's Law with $T_\mu = 273$, $S_\mu = 111$, and $\mu_0 = 1.716 \times 10^{-5}$:

$$\mu = \mu_0 \frac{T_\mu + S_\mu}{T + S_\mu} \left(\frac{T}{T_\mu} \right)^{\frac{3}{2}} \quad (3.12)$$

$$\mu = \frac{\mu_0(T_\mu + S_\mu)}{T_\mu^{\frac{3}{2}}} \frac{T_0^{\frac{3}{2}} F^{-\frac{3}{2}}}{T_0 F^{-1} + S_\mu} \quad (3.13)$$

$$\frac{\frac{d\mu}{dt}}{\mu} = (\gamma - 1)MF^{-1} \frac{dM}{dt} \left(\frac{T_0 F^{-1}}{T_0 F^{-1} + S_\mu} - \frac{3}{2} \right) \quad (3.14)$$

Substituting and solving for $\frac{dP_0}{dt}$:

$$\frac{dP_0}{dt} = P_0 MF^{-1} \frac{dM}{dt} \left[(\gamma - 1) \left(\frac{T_0 F^{-1}}{T_0 F^{-1} + S_\mu} - \frac{3}{2} \right) + \frac{\gamma+1}{2} - \frac{1}{M^2 F^{-1}} \right] \quad (3.15)$$

end{fix equations}

Following the same logic as before, either a PI, PID, or PID with high frequency noise filtering will be implemented based on experimental results of Reynolds number control. However, in this case the calculated Reynolds number will be subtracted from the set condition to get the error signal and the controlled parameter will either be the stagnation pressure or the respective regulator position.

$$E(s) = Re'_{\text{set}} - Re'(s) \quad (3.16)$$

$$G(s) = \frac{P_0(s)}{E(s)} \text{ or } \frac{X(s)}{E(s)} = K \left(1 + \frac{1}{T_i s} \right) \quad (3.17a)$$

$$= K \left(1 + \frac{1}{T_i s} + T_d s \right) \quad (3.17b)$$

$$= K \left(1 + \frac{1}{T_i s} + \frac{T_d s}{1 + \frac{T_d s}{N}} \right), \quad N = 2 \text{ to } 20 \quad (3.17c)$$

At the very least, this model will be fully developed and simulated to ensure minimal future work for implementation. The physical control mechanism will also be explored and potentially purchased to allow install at the earliest convenience between the ACE2.0 and M6QT schedules.

3.2 Freestream Pressure Fluctuation Levels and Uniformity Characterization

In order to establish a baseline of performance characteristics for future work within the ACE2.0 facility, a pitot survey will be performed to measure and characterize the freestream flow uniformity and pressure fluctuation levels (noise) throughout the nozzle. The survey will utilize both a single pitot probe and a pitot rake with Kulite pressure transducers mounted on a traverse to characterize the entire nozzle exit plane and centerline up to 24 inches upstream of the nozzle exit.

A final noise survey was performed in ACE to establish a control for comparison with ACE2.0 as well as provide a preliminary exploration of noise hysteresis. The survey utilized a single pitot probe to measure the noise along the centerline at four different axial locations: 0, 6, 17, and 24 inches upstream of the nozzle exit. For each run, the Reynolds number was increased above the transition value ($Re' = 3 \times 10^6 / m$) discussed in the previous chapter and then decreased back down to the initial value below the transition value. This process provided baseline data for pressure fluctuation hysteresis. The results are shown in Figure 3.1. As seen, there is no discernible hysteresis in the freestream pressure fluctuation levels as the Reynolds number is swept up and back down.

The anticipated characterization test matrix options for ACE2.0 are shown in Tables ?? and 3.1. These test matrix options are for the unavailability and availability of a pitot rake, respectively. The



Figure 3.1: ACE freestream pressure fluctuations...

functionality of the pitot rake is currently unknown, but it would provide simultaneous measurements across the y-axis and allow Mach number to be efficiently added as an extra dimension of uniformity. The runs in each test matrix are divided into a few distinct objectives: (1) uniformity, (2) uncertainty quantification, (3) pressure fluctuation levels transition, and (4) hysteresis. The last set of runs will be replicates of the first set to quantify the uncertainty in Mach number, Reynolds number, and flow uniformity.

3.2.1 Freestream Uncertainty Quantification

The process to quantify the uncertainty of the various parameters for this work will closely follow Stephens's et al. [31] and Curriston's [32] approaches by simply focusing on establishing a baseline for the uncertainty and making recommendations for improvement if necessary. The three steps to establish this baseline uncertainty for ACE2.0 will be (1) gather/measure systematic



Figure 3.2: Pitot probe measuring 17 inches upstream of nozzle exit.

elemental uncertainties, (2) input into a Monte Carlo code along with data reduction equations to simulate systematic uncertainties, and (3) measure repeat data points through a few replicate experiments and calculate random uncertainties.

First, the systematic elemental uncertainties can be gathered and measured from the various sensors, which includes the static pressure transducer, stagnation pressure transducer, stagnation temperature thermocouple, and servo motor internal encoders. Each of these has a predefined manufacturer uncertainty that can be used, but some of these are very conservative and not ideal. The pressure sensors and temperature sensor will be tested against a working standard to measure the true uncertainty, which is often found to be an order of magnitude less than the manufacturer uncertainty [32]. The systematic uncertainty of any sensors utilized in future experiments is outside the scope of this work and must be considered when calculating the total uncertainty of measurements

Run	X (in.)	Y (in.)	Z (in.)	Mach	$Re' (10^6)$	Instrument
1	0	-3:1:3	0	6*	3*	Rake
2	0	-3:1:3	-3:1:3	8	3	Rake
3	0	-3:1:3	-3:1:3	7	3	Rake
4	0	-3:1:3	-3:1:3	6	3	Rake
5	0	-3:1:3	-3:1:3	5	3	Rake
6	-6	-3:1:3	-3:1:3	5	3	Rake
7	-6	-3:1:3	-3:1:3	6	3	Rake
8	-6	-3:1:3	-3:1:3	7	3	Rake
9	-6	-3:1:3	-3:1:3	8	3	Rake
10	0	0	0	8	2→7→2	Pitot
11	0	0	0	7	2→7→2	Pitot
12	0	0	0	6	2→7→2	Pitot
13	0	0	0	5	2→7→2	Pitot
14	0	0	0	5→8→5	3	Pitot
15	-6	0	0	5→8→5	3	Pitot
16	-6	0	0	5	2→7→2	Pitot
17	-6	0	0	6	2→7→2	Pitot
18	-6	0	0	7	2→7→2	Pitot
19	-6	0	0	8	2→7→2	Pitot
20	-17	0	0	6	2→7→2	Pitot
21	-17	0	0	5→8→5	3	Pitot
22	-24	0	0	5→8→5	3	Pitot
23	-24	0	0	6	2→7→2	Pitot
24-37	Repeat runs 10-23 with Hot-wire					
38-42	Replicate runs 1-5					

Table 3.1: Test matrix for ACE2.0 freestream characterization.

in each experiment.

Next, these systematic elemental uncertainties will be propagated through a Monte Carlo simulation along with the specific data reduction equations for the facility. This output will provide the total systematic uncertainty for each parameter of interest, which will be added to the random uncertainty to give the total uncertainty. Additionally, this simulation will also be used to provide a sensitivity analysis of the uncertainty to the various input parameters. This will be insightful on how to best improve the uncertainty if necessary.

Finally, repeat data points will be measured by repeatedly settling on and off the set condition

for the parameter of interest. While data will be gathered throughout the entire characterization test matrix, runs 1 and 20 will be solely for repeat data measurements. These two runs will provide a direct comparison of replicates that will account for any correlations that were not considered or unquantifiable. The standard deviation of this data will be added in quadrature to the systematic uncertainty to calculate the total uncertainty for each parameter of interest for the freestream flow.

3.2.2 Freestream Hysteresis

Dynamic sweeps of both Mach number and Reynolds number will be performed to explore any potential hysteresis effects in either the noise or the control parameters. Specifically, this will be accomplished during the dynamic runs in the characterization test matrix in Table 3.1. The goal is simply to identify the existence of any hysteresis effects to inform future work within ACE2.0. The Reynolds number sweep runs are necessary to determine the value at which transition occurs, so sweeping the Reynolds number back down will not add any additional work and will ensure that there is no hysteresis. For the Mach number however, there is no past data to determine the existence of hysteresis, so these runs will establish a baseline. The noise level is known to decrease with an increase in Mach number, so identifying an hysteresis in this will be necessary to inform future experiments.

3.3 Mach Trajectory and Potential Hysteresis Proof of Concept Experiment

This objective will primarily serve as a demonstration of the capabilities for ACE2.0 and will also provide preliminary insight into the hysteretic behavior of dynamic Mach number experiments. The flow characteristic that will be specifically explored in this research will be shock interactions using schlieren. The goal will be to observe hysteresis in the transition from regular reflection to Mach reflection by varying the Mach number. The challenge of this is that the only facilities that have successfully produced this hysteresis were low-noise with an open, free-jet test section, while ACE2.0 has a closed test section and is not expected to be a low-noise facility.

The experiments will be based on the methodologies and results from Durand et al. [15] and Tao et al. [45] in addition to the experimental setup of Mai [6]. The Mach number will be varied across

either the Von Neumann condition or the detachments criteria to force the transition from regular reflection to Mach reflection or vice versa. In order to choose the wedge angle and Mach number range for each experiment, Figure 3.6 was created following the processes shown by Mouton [42] for each condition. The basic parameters across an oblique shock shown in Figure 3.3 are given as a function of the Mach number in region x (M_x), the shock angle (α), and the ratio of specific heats (γ).

Too much in the weeds. Reword as just process? without all the equations

The pressure ratio is

$$\xi(M_x, \alpha) = \frac{P}{P_x} = \frac{2\gamma M_x^2 \sin^2 \alpha - (\gamma - 1)}{\gamma + 1} \quad (3.18)$$

The flow deflection angle (wedge angle) and Mach number are given as

$$\theta(M_x, \alpha) = \cot^{-1} \left[\left(\frac{(\gamma + 1)M_x^2}{2(M_x^2 \sin^2 \alpha - 1)} \right) \tan \alpha \right] \quad (3.19)$$

$$M(M_x, \alpha) = \sqrt{\frac{(\gamma + 1)^2 M_x^4 \sin^2 \alpha - 4(M_x^2 \sin^2 \alpha - 1)(\gamma M_x^2 \sin^2 \alpha + 1)}{[2\gamma M_x^2 \sin^2 \alpha - (\gamma - 1)][(\gamma - 1)M_x^2 \sin^2 \alpha + 2]}} \quad (3.20)$$

The shock angle when the flow deflection angle is maximum is given by setting $\frac{\partial \theta}{\partial \alpha} = 0$, resulting in

$$\alpha^{\theta_{max}}(M_x) = \sin^{-1} \sqrt{(\gamma + 1) \frac{M_x^2 - \frac{4}{\gamma+1} + \sqrt{M_x^4 + 8\frac{\gamma-1}{\gamma+1}M_x^2 + \frac{16}{\gamma+1}}}{4\gamma M_x^2}} \quad (3.21)$$

For the detachment condition shown in Figure 3.3

$$M_{1,D} = M(M_\infty, \alpha_D) \quad (3.22)$$

$$\theta(M_\infty, \alpha_D) = \theta(M_{1,D}, \alpha^{\theta_{max}}(M_{1,D})) \quad (3.23)$$

Solving this for α_D results in a fifth-order polynomial in $\sin^2 \alpha_D$

$$D_0 + D_1 \sin^2 \alpha_D + D_2 \sin^4 \alpha_D + D_3 \sin^6 \alpha_D + D_4 \sin^8 \alpha_D + D_5 \sin^{10} \alpha_D = 0 \quad (3.24)$$

where

$$D_0 = -16$$

$$D_1 = 32M_\infty^2 - 4M_\infty^4 - 48M_\infty^2\gamma - 16M_\infty^4\gamma + 16\gamma^2 - 16M_\infty^4\gamma^2$$

$$+ 16M_\infty^2\gamma^3 + 4M_\infty^4\gamma^4$$

$$D_2 = -16M_\infty^4 + 4M_\infty^6 - M_\infty^8 + 104M_\infty^4\gamma + 16M_\infty^6\gamma - 4M_\infty^8\gamma$$

$$- 64M_\infty^2\gamma^2 - 32M_\infty^4\gamma^2 + 8M_\infty^6\gamma^2 - 6M_\infty^8\gamma^2 - 56M_\infty^4\gamma^3$$

$$- 16M_\infty^6\gamma^3 - 4M_\infty^8\gamma^3 - 12M_\infty^6\gamma^4 - M_\infty^8\gamma^4$$

$$D_3 = M_\infty^8 - 64M_\infty^6\gamma + 4M_\infty^8\gamma + 96M_\infty^4\gamma^2 + 64M_\infty^6\gamma^2 + 14M_\infty^8\gamma^2$$

$$+ 64M_\infty^6\gamma^3 + 20M_\infty^8\gamma^3 + 9M_\infty^8\gamma^4$$

$$D_4 = 8M_\infty^8\gamma - 64M_\infty^6\gamma^2 - 32M_\infty^8\gamma^2 - 24M_\infty^8\gamma^3$$

$$D_5 = 16M_\infty^8\gamma^2$$

This equation is solved numerically for Mach numbers greater than unity, and only one solution for each $\sin^2 \alpha_D$ exists that is real and bounded between zero and one. The values of $\theta_D(M) = \theta(M_\infty, \alpha_D)$ solved for freestream Mach numbers from 2 to 9 yields the upper curve in Figure 3.6.

For the Von Neumann condition shown in Figure 3.4

$$M_{1,V} = M(M_\infty, \alpha_V) \quad (3.25)$$

$$\xi\left(M_\infty, \frac{\pi}{2}\right) = \xi(M_\infty, \alpha_V) \xi(M_{1,V}, \alpha_{1,V}) \quad (3.26)$$

$$\frac{2\gamma M_{1,V}^2 \sin^2 \alpha_{1,V} - (\gamma - 1)}{\gamma + 1} = \frac{\xi(M_\infty, \frac{\pi}{2})}{\xi(M_\infty, \alpha_V)} \quad (3.27)$$

$$\alpha_{1,V} = \sin^{-1} \sqrt{\frac{(\gamma - 1) + (\gamma + 1) \frac{\xi(M_\infty, \frac{\pi}{2})}{\xi(M_\infty, \alpha_V)}}{2\gamma M_{1,V}^2}} \quad (3.28)$$

The solution for $\alpha_{1,V}$ is found numerically by solving the equation

$$\theta(M_\infty, \alpha_V) = \theta(M_{1,V}, \alpha_{1,V}) \quad (3.29)$$

The values of $\theta_V(M) = \theta(M_\infty, \alpha_V)$ solved for freestream Mach numbers from 2.2 to 9 yields the lower curve in Figure 3.6.

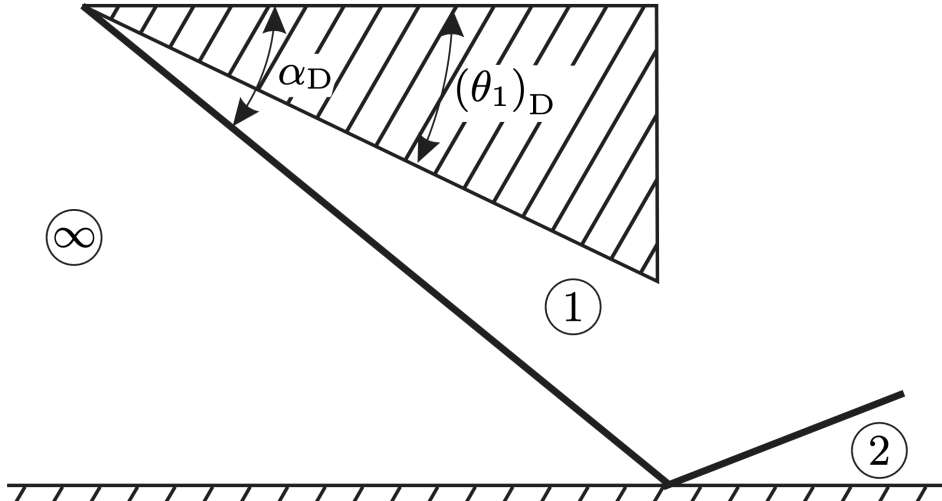


Figure 3.3: Flow over wedge resulting in regular reflection of shock [42]

The two experimental setups are shown as A and B. For A, the wedge angle is 29.4° and the Mach number range is 6 to 7. For B, the wedge angle is 20.4° and the Mach number range is 5.5 to 7.5. For both paths, the Mach number will start at the point in the dual solution domain, decrease across either the detachment condition or the Von Neumann condition, and then increase back into the dual solution domain (i.e. AA'A, BB'B). The reverse of these will also be explored if hysteresis

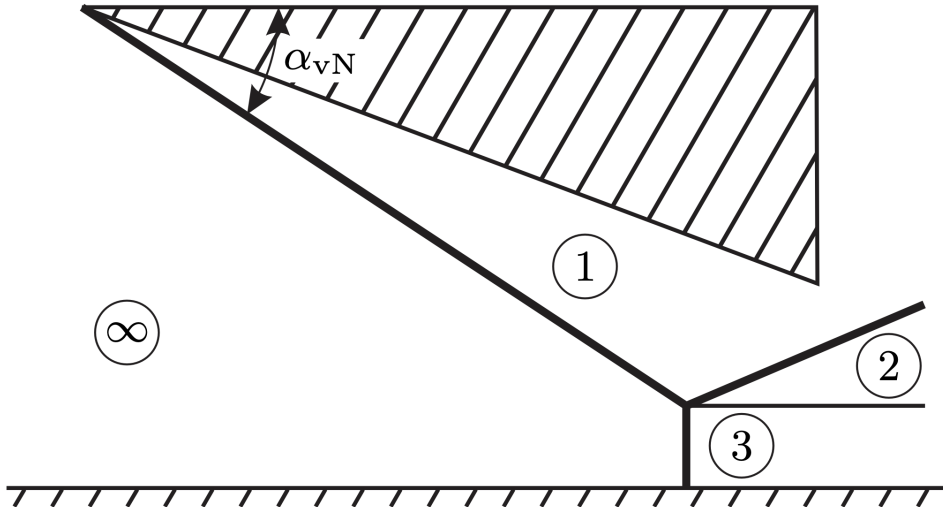


Figure 3.4: Flow over wedge resulting in Mach reflection of shock [42]

is not observed initially.

The physical model for these experiments will be very similar to the double wedge setup used by Mai [6] in ACE as shown in Figure 3.5. If 3D printing with Rigid 10K produces acceptable wedges, then a pair will be printed for each angle needed. If future research will utilize this double wedge setup, then a hinged mechanism will be designed and fabricated to use a single pair of wedges for any desired angle.

The expected results should appear similar to the numerical results by Ben-Dor et al. [37] shown in Figure 3.7. Although the Mach number range is different, the hysteresis should be the same for the chosen paths in this experiment. This path in this simulation is representative of path AA'A, which crosses the detachment condition. There have not been any simulations published that cross the Von Neumann condition by varying the Mach number, so path B will be explored secondary to path A.

In either case, the final objective will be to guide future experiments by determining if ACE2.0 is capable of reproducing the hysteresis in shock interactions or incapable due to freestream noise.

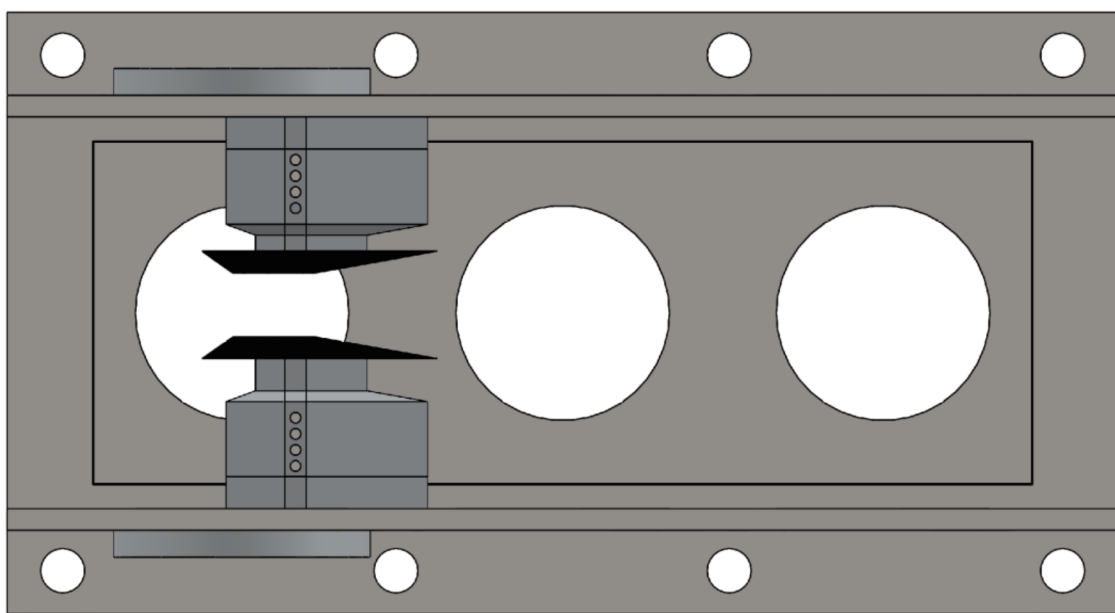


Figure 3.5: Double wedge setup [6]

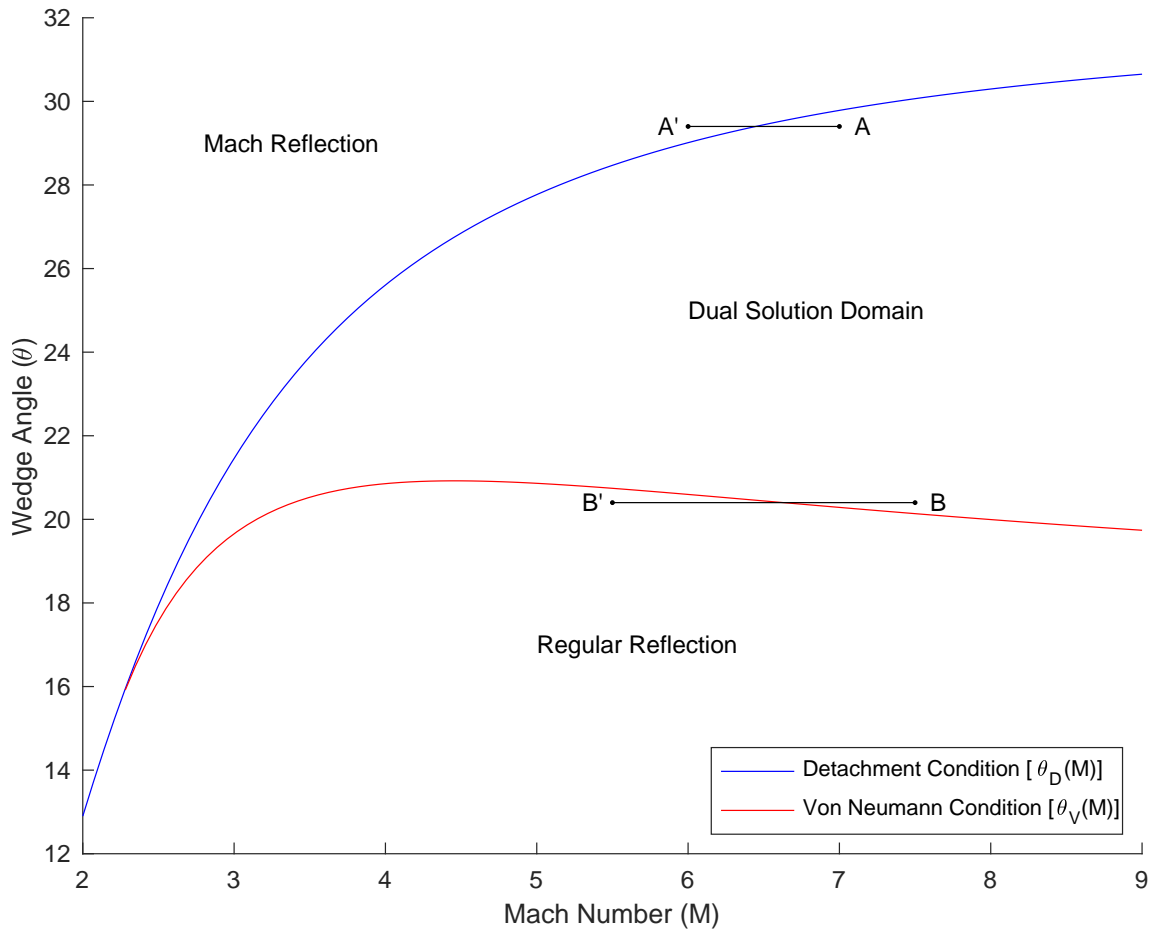


Figure 3.6: Shock wave reflection configuration domains for Mach number and wedge angle.

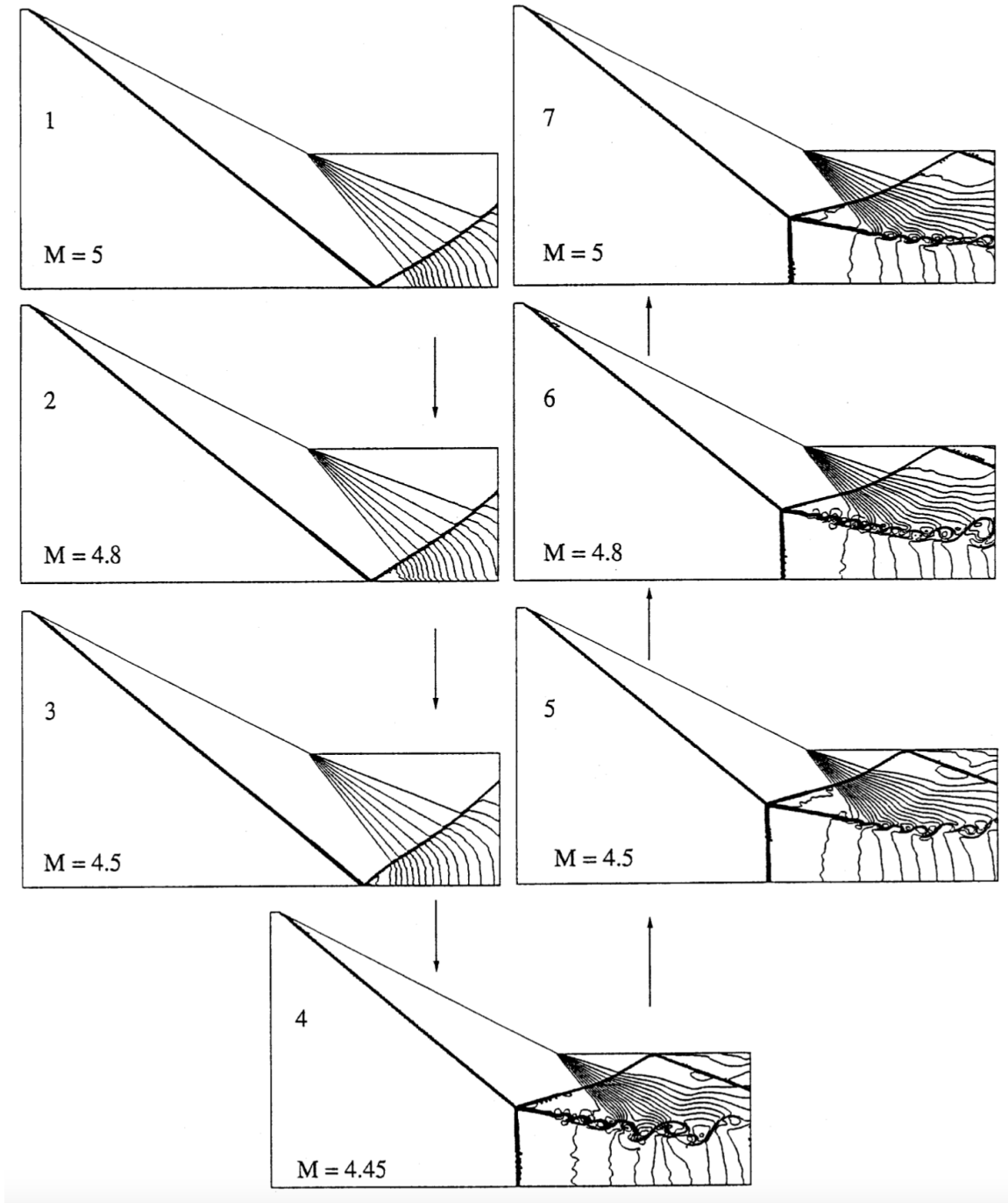


Figure 3.7: Mach-number-variation-induced hysteresis for 27° wedge [37]

4. REAMAINING WORK

The path forward will follow the manufacturing schedule shown in Figure 2.20. The pressure test will be performed as soon as the nozzles are finished machining, tentatively May 1, 2024. Depending on the results of the pressure test, the process could be anywhere from a single day to two weeks. Once complete though, the nozzles and sidewalls will be shipped to the polishing vendor, which should have a quick turn around of two weeks. Upon arrival to the NAHL, the full ACE2.0 nozzle will be finally assembled and installed. With proper planning prior to the final installation, the process should not take more than a week to begin shakedown and characterization.

In the meantime, the servo control program will be written between now and the final nozzle machining. The Mach number feedback will be implemented, and the Reynolds number control capability will be explored and potentially implemented before the final install. Again, this will primarily depend on the test schedule for the M6QT and the amount of time needed to replace the manual valve with a controlled valve.

The characterization and hysteresis experiments will be performed immediately following installation and initial calibration. The primary goal is to ensure complete function of ACE2.0 along with a demonstration of the capabilities and potential for future research. Additionally, the documentation for the nozzle operation will be written based on the best practices deduced throughout the experiments.

4.1 Maybe

Might have another section

4.2 Possibly

Could possibly have another section

REFERENCES

- [1] I. A. Leyva, “The relentless pursuit of hypersonic flight,” *Physics Today*, vol. 70, pp. 30–36, 11 2017.
- [2] M. Semper, N. Tichenor, R. Bowersox, R. Srinivasan, and S. North, *On the Design and Calibration of an Actively Controlled Expansion Hypersonic Wind Tunnel*.
- [3] N. Tichenor, M. Semper, R. Bowersox, R. Srinivasan, and S. North, *Calibration of an Actively Controlled Expansion Hypersonic Wind Tunnel*.
- [4] N. Tichenor, *Characterization of the Influence of a Favorable Pressure Gradient on the Basic Structure of a Mach 5.0 High Reynolds Number Supersonic Turbulent Boundary Layer*. Doctoral dissertation, Texas A&M University, 2010.
- [5] M. Semper, B. Pruski, and R. Bowersox, *Freestream Turbulence Measurements in a Continuously Variable Hypersonic Wind Tunnel*.
- [6] C. Mai, *Near-Region Modification of Total Pressure Fluctuations by a Normal Shock Wave in a Low-Density Hypersonic Wind Tunnel*. Doctoral dissertation, Texas A&M University, 2014.
- [7] I. Neel, *Influence of Environmental Disturbances on Hypersonic Crossflow Instability on the HIFiRE-5 Elliptic Cone*. Doctoral dissertation, Texas A&M University, 2019.
- [8] A. N. Leidy, *An Experimental Characterization of 3-D Transitional Shock Wave Boundary Layer Interactions at Mach 6*. PhD thesis, 2019.
- [9] J. T. Kenney and L. M. Webb, “A summary of the techniques of variable mach number supersonic wind tunnel nozzle design,” *AGARDograph*, no. 3, 1954.
- [10] J. Rosen, “The design and calibration of a variable mach number nozzle,” *Journal of the Aeronautical Sciences*, vol. 22, no. 7, pp. 484–490, 1955.

- [11] S. F. Erdmann, “A new economic flexible nozzle for supersonic wind tunnels,” *Journal of Aircraft*, vol. 8, no. 1, pp. 58–60, 1971.
- [12] J. Rom and I. Etsion, “Improved flexible supersonic wind-tunnel nozzle operated by a single jack.,” *AIAA Journal*, vol. 10, no. 12, pp. 1697–1699, 1972.
- [13] B. Ilic, M. Milos, M. Milosavljevic, and J. Isakovic, “Model-based stagnation pressure control in a supersonic wind tunnel,” *FME Transaction*, vol. 44, pp. 1–9, 01 2016.
- [14] A. N. Shahrabaki, M. Bazazzadeh, M. D. Manshadi, and A. Shahriari, “Designing a fuzzy logic controller for the reynolds number in a blowdown supersonic wind tunnel,” *2014 IEEE Aerospace Conference*, pp. 1–12, 2014.
- [15] A. Durand, B. Chanetz, R. Benay, and A. Chpoun, “Investigation of shock waves interference and associated hysteresis effect at variable-mach-number upstream flow,” *Shock Waves*, vol. 12, p. 469–477, May 2003.
- [16] L. Laguarda, J. Santiago Patterson, F. F. Schrijer, B. W. van Oudheusden, and S. Hickel, “Experimental investigation of shock–shock interactions with variable inflow mach number,” *Shock Waves*, vol. 31, p. 457–468, Jul 2021.
- [17] P. Chen, F. Wu, J. Xu, X. Feng, and Q. Yang, “Design and implementation of rigid-flexible coupling for a half-flexible single jack nozzle,” *Chinese Journal of Aeronautics*, vol. 29, no. 6, pp. 1477–1483, 2016.
- [18] S.-g. Guo, Z.-g. Wang, and Y.-x. Zhao, “Design of a continuously variable mach-number nozzle,” *Journal of Central South University*, vol. 22, p. 522–528, Feb 2015.
- [19] Z. Lv, J. Xu, F. Wu, P. Chen, and J. Wang, “Design of a variable mach number wind tunnel nozzle operated by a single jack,” *Aerospace Science and Technology*, vol. 77, pp. 299–305, 2018.
- [20] W. Qi, J. Xu, and Z. Fan, *Design and Experimental Calibration of the Profile Rotating Wind Tunnel with Mach Number Varying from 2.0 to 4.0*.

- [21] C. A. Steeves, K. H. Timpano, P. T. Maxwell, L. Martinelli, and R. B. Miles, “Design and manufacture of a morphing structure for a shape-adaptive supersonic wind tunnel nozzle,” *Journal of Applied Mechanics*, vol. 76, no. 3, p. 031012, 2009.
- [22] D. Kraft, “Optimal control of a high performance wind tunnel,” *IFAC Proceedings Volumes*, vol. 18, no. 2, pp. 233–234, 1985. 5th IFAC Workshop on Control Applications of Nonlinear Programming and Optimization, Capri, Italy, Capri, Italy.
- [23] D.-S. Hwang and P.-L. Hsu, “A robust controller design for supersonic intermittent blowdown-type windtunnels,” *The Aeronautical Journal*, vol. 102, no. 1013, p. 161–170, 1998.
- [24] J. Matsumoto, F. Lu, and D. Wilson, “Pre-programmed controller for a supersonic blowdown tunnel,” 01 2001.
- [25] Y. T. Fung, G. Settles, and A. Ray, *Microprocessor Control of High-Speed Wind Tunnel Stagnation Pressure*.
- [26] B. Ilić, M. Miloš, and J. Isaković, “Cascade nonlinear feedforward-feedback control of stagnation pressure in a supersonic blowdown wind tunnel,” *Measurement*, vol. 95, pp. 424–438, 2017.
- [27] M. G. Silva, V. O. Gamarra, and V. Koldaev, “Control of reynolds number in a high speed wind tunnel,” *Journal of Aerospace Technology and Management*, vol. 1, pp. 69–77, 2009.
- [28] C. Nott, S. Ölçmen, D. Lewis, and K. Williams, “Supersonic, variable-throat, blow-down wind tunnel control using genetic algorithms, neural networks, and gain scheduled pid,” *Appl. Intell.*, vol. 29, pp. 79–89, 08 2008.
- [29] A. Chou, A. Leidy, R. A. King, B. F. Bathel, and G. Herring, *Measurements of Freestream Fluctuations in the NASA Langley 20-Inch Mach 6 Tunnel*.
- [30] L. Duan, M. M. Choudhari, A. Chou, F. Munoz, R. Radespiel, T. Schilden, W. Schröder, E. C. Marineau, K. M. Casper, R. S. Chaudhry, G. V. Candler, K. A. Gray, and S. P. Schnei-

- der, “Characterization of freestream disturbances in conventional hypersonic wind tunnels,” *Journal of Spacecraft and Rockets*, vol. 56, no. 2, pp. 357–368, 2019.
- [31] J. Stephens, E. Hubbard, J. Walter, and T. McElroy, “Uncertainty analysis of the nasa glenn 8x6 supersonic wind tunnel,” tech. rep., 2016.
- [32] D. Curriston, *Wind Tunnel Data Quality Assessment and Improvement Through Integration of Uncertainty Analysis in Test Design*. Doctoral dissertation, Texas A&M University, 2024.
- [33] H. G. Hornung, H. Oertel, and R. J. Sandeman, “Transition to mach reflexion of shock waves in steady and pseudosteady flow with and without relaxation,” *Journal of Fluid Mechanics*, vol. 90, no. 3, p. 541–560, 1979.
- [34] H. G. Hornung and M. L. Robinson, “Transition from regular to mach reflection of shock waves part 2. the steady-flow criterion,” *Journal of Fluid Mechanics*, vol. 123, p. 155–164, 1982.
- [35] A. Chpoun and G. Ben-Dor, “Numerical confirmation of the hysteresis phenomenon in the regular to the mach reflection transition in steady flows,” *Shock Waves*, vol. 5, pp. 199–203, 1995.
- [36] M. Ivanov, G. Ben-Dor, T. Elperin, A. Kudryavtsev, and D. Khotyanovsky, “Flow-mach-number-variation-induced hysteresis in steady shock wave reflections,” *AIAA journal*, vol. 39, no. 5, pp. 972–974, 2001.
- [37] G. Ben-Dor, M. Ivanov, E. Vasilev, and T. Elperin, “Hysteresis processes in the regular reflection mach reflection transition in steady flows,” *Progress in Aerospace Sciences*, vol. 38, no. 4-5, pp. 347–387, 2002.
- [38] A. Chpoun, D. Passerel, H. Li, and G. Ben-Dor, “Reconsideration of oblique shock wave reflections in steady flows. part 1. experimental investigation,” *Journal of Fluid Mechanics*, vol. 301, p. 19–35, 1995.
- [39] G. Ben-Dor and G. Ben-Dor, *Shock wave reflection phenomena*, vol. 2. Springer, 2007.

- [40] H. LI, A. CHPOUN, and G. BEN-DOR, “Analytical and experimental investigations of the reflection of asymmetric shock waves in steady flows,” *Journal of Fluid Mechanics*, vol. 390, p. 25–43, 1999.
- [41] M. S. Ivanov, A. N. Kudryavtsev, S. B. Nikiforov, D. V. Khotyanovsky, and A. A. Pavlov, “Experiments on shock wave reflection transition and hysteresis in low-noise wind tunnel,” *Physics of Fluids*, vol. 15, pp. 1807–1810, 06 2003.
- [42] C. A. Mouton, *Transition between regular reflection and Mach reflection in the dual-solution domain*. PhD thesis, California Institute of Technology, 2007.
- [43] T. Setoguchi, S. Matsuo, M. Ashraful Alam, J. Nagao, and H. D. Kim, “Hysteretic phenomenon of shock wave in a supersonic nozzle,” *Journal of Thermal Science*, vol. 19, pp. 526–532, 2010.
- [44] B. Chanetz and R. Benay, “Hysteresis phenomena associated with shock waves interference in steady hypersonic flow,” *International Journal of Aerodynamics*, vol. 2, no. 2-4, pp. 294–315, 2012.
- [45] Y. Tao, X. Fan, and Y. Zhao, “Viscous effects of shock reflection hysteresis in steady supersonic flows,” *Journal of fluid mechanics*, vol. 759, pp. 134–148, 2014.
- [46] K. Sabnis, D. Galbraith, H. Babinsky, and J. A. Benek, *The Influence of Nozzle Geometry on Corner Flows in Supersonic Wind Tunnels*.
- [47] W. S. Saric, “Görtler vortices,” *Annual Review of Fluid Mechanics*, vol. 26, no. 1, pp. 379–409, 1994.
- [48] E. Reshotko, W. Saric, and H. Nagib, “Flow quality issues for large wind tunnels,” *35th Aerospace Sciences Meeting and Exhibit*, Jan 1997.
- [49] W. F. Hilton, “High speed wind tunnel testing. a. pope and k. l. goin. john wiley & sons, london. 1965. 474 pp. illustrations. 115s.,” *The Aeronautical Journal*, vol. 70, no. 667, p. 739–739, 1966.

- [50] J. Anderson, *Fundamentals of Aerodynamics*. McGraw-Hill series in aeronautical and aerospace engineering, McGraw-Hill Education, 2017.
- [51] J. Anderson, *Modern Compressible Flow: With Historical Perspective*. Aeronautical and Aerospace Engineering Series, McGraw-Hill Education, 2021.

APPENDIX A

ACE2.0 NOZZLE CONTOUR

Code and equations to produce contour

Before:

```
do 10 i=1, nch
    theta(i) = dthetai + float(i-1)*dth
    x(i) = tan(theta(i))/2./k
    xw(i) = x(i)
    y(i) = 1.0 + k*x(i)**2
    yw(i) = y(i)
10 continue
```

After:

```
do 10 i=1, nch
    theta(i) = dthetai + float(i-1)*dth
    xthetai = sqrt(tan(thetai)/k)
    k4 = -k/2./xthetai
    pc = -9.* (k**2)/3. / ((4.*k4)**2)
    qc = (2.* (3.*k)**3 - 27.* ((4.*k4)**2)*tan(theta(i)))
    & / 27. / ((4.*k4)**3)
    npi = 2.*pi/3.
    tc = 2.*sqrt(-pc/3.)
    & *cos(acos((3.*qc/2./pc)*sqrt(-3./pc))/3. - npi)
    if((3.*qc/2./pc)*sqrt(-3./pc).lt.-1.) then
        tc = 2.*sqrt(-pc/3.)*cos(acos(-1.)/3. - npi)
    end if
    x(i) = tc - k/4./k4
    xw(i) = x(i)
    y(i) = 1.0 + k*x(i)**3 + k4*x(i)**4
    yw(i) = y(i)
10 continue
```

The equations for each section are given by the following (in inches):

Subsonic: $-0.000267975228779994x^5 - 0.0066993807195x^4 - 0.04466253813x^3 + 0.033746187$

for $-10 < x < 0$

Throat: $-2689.610971179115x^4 + 181.528229581324x^3 + 0.033746187$ *for* $0 < x < 0.033746187$

Straight: $0.206725280364801x + 0.030258092015591$ *for* $0.033746187 < x < 6.1460114$

Straightening: $2.180909737850381x^{0.960492634168194} + 5.934566177927477 \times 10^{284}x^{-367.9331632104439}$
 $-1.684363604007221x^{1.011336503949665} - 0.023814395465567 \ln(0.418646933043039x)$
 -0.585293189697896 for $6.1460114 < x < 40.07774$



Figure A.1: A caption here

APPENDIX B

CFD RESULTS

The following figures show the full results compared between ACE and ACE2.0.



Figure B.1: A caption here

APPENDIX C
ACTUATION SPECIFICATIONS

Text for the Appendix follows.



Figure C.1: A caption here

C.1 Appendix Section

C.2 Another Appendix Section